Strål
säkerhets
myndigheten
Swedish Radiation Safety Authority

Research

Computational analysis of high-burnup fuel rod behaviour in PWR large-break LOCA

2024:10

Author: Lars Olof Jernkvist, Quantum Technologies AB, Uppsala
Date: June, 2024
Report number: 2024:10
ISSN: 2000-0456
Available at www.ssm.se

Strål
säkerhets
myndigheten
Swedish Radiation Safety Authority

Author: Lars Olof Jernkvist, Quantum Technologies AB, Uppsala

2024:10

Computational analysis of high-burnup fuel rod behaviour in PWR large-break LOCA

Date: June, 2024
Report number: 2024:10
ISSN: 2000-0456
Available at www.stralsakerhetsmyndigheten.se

This report was commissioned by the Swedish Radiation Safety Authority (SSM). The conclusions and viewpoints presented in the report are those of the author(s) and do not necessarily coincide with those of SSM.

SSM perspective

Background

Quantum Technologies AB (QT) has for many years developed computational models for the thermomechanical behaviour of nuclear fuel in events such as LOCA and RIA. The research projects have been based on evaluations of tests on nuclear fuel in Halden Reactor Project (HRP) and Studsvik Cladding Integrity Project (SCIP). The models developed by QT enable analyses and interpretations of the tests, including the analysis of new phenomena such as fuel fragmentation and its impact on the damage process.

In this research project, a newly developed version of FRAPTRAN has been used for more realistic analyses of the events experienced by several fuel rods during a LOCA. In collaboration with Ringhals AB and Vattenfall Nuclear Fuel AB (VNF), QT has analysed 50 fuel rods with high burnup and how they could behave in a LOCA. Thermal-hydraulic boundary conditions (scenario and heat transfer coefficient) have been taken from a work done at Chalmers University of Technology as part of a previous research assignment for SSM (SSM2014-1043-15). VNF has selected rods and produced power histories for the rods to use as initial values in the calculations of the LOCA process.

Results

The results show that even though several of the rods in the study reach conditions that result in fragmentation and relocation of the fuel, only a few of these rods experience cladding failure. The fragmentation and relocation of the pellets leads to several effects on the fuel, primarily a temperature increase which in turn drives oxidation and cladding temperature. Cladding failure is obtained in this analysis due to oxidation and stress conditions in the cladding in the later stage of the event.

The choice of scenario has an impact on the calculated damage process; the rods that are expected to be damaged are so in the later part of the event. In the current work, a “cladding damage index” has also been produced which shows that in the course of the event several rods are close to damage in the earlier part of the event. None of the rods experience damage in the early part of the event in the current scenario but minor changes to the scenario can lead to other causes of damage and possibly more severe consequences of the event.

It is noted that no significant effect is seen on the rods with an initial linear heat generation rate of less than 15 kW/m, suggesting that the behaviour of the fuel is largely dependent on its power. Power level seems to be a more important parameter than e.g. burnup.

All in all, it can be concluded that for a realistic case, which however has some conservative boundary values, there does not seem to be extensive damage to the fuel, nor the consequences with the release of fission gases and pellet fragments. Fragmentation in high burn-up fuel can occur without causing damage. By understanding which phenomena are most significant, strategies can also be developed to mitigate the process based on these phenomena.

Relevance

This research project has provided an insight into the conditions for the nuclear fuel in Ringhals in a LOCA, taking into account phenomena studied in recent years (fuel fragmentation). The research project has provided further in-depth input to

SSM's work in the supervision of the safety assessment for the reactors at Ringhals. This work and its conclusions can complement the previous review in SSM2014-1043-4 " Granskning inför beslut om godkännande av förnyad SAR och ansökan om provdrift vid 3300 MW termisk effekt för Ringhals 4" and specifically the expectations expressed by SSM in Action 9 to investigate the extent of the impact on the fuel in the analyses for loss of coolant for the power-increased reactor. This current research project indicates that the operation of the Ringhals reactors is such that only a limited amount of fuel rods risk damage during a LOCA. However, only one LOCA scenario has been studied here and small changes in the scenario can lead to other effects in the fuel. It should also be considered that the fuel rods in the study were chosen by Ringhals.

Need for further research

As the fuel is developed and tested under new conditions, new phenomena are observed. Analyses and interpretations of the tests are very valuable in understanding the phenomena present in the tests, and what may be driving an event. Based on this knowledge, limits can be determined and analyses improved. It is important that the tests continue and that SSM has support for analyses and interpretations of the tests.

Project information

Contact person SSM: Cheuk Lau
Reference: SSM2022-3726 / 4530512

Computational analysis of high-burnup fuel rod behaviour in PWR large-break LOCA

Lars Olof Jernkvist

Quantum Technologies AB

Contents

List of appendices

Appendices C and D contain confidential information and are not included in the public version of the report.

Summary

This report deals with an *in-silico* study, in which the thermal-mechanical behaviour of high-burnup UO_2 fuel rods under a postulated large-break loss-of-coolant accident (LB LOCA) in a pressurized water reactor (PWR) is simulated by use of state-of-the-art computational models. The study aims to assess to what extent certain high-burnup phenomena, observed in experiments under non-prototypical conditions, are manifested in current design fuel rods that undergo a typical PWR design-basis LB LOCA at end of their service life.

The high-burnup phenomena of interest are fuel pellet fine fragmentation, transient fission gas release in combination with restricted axial gas flow, axial relocation of fragmented fuel, and dispersal of fuel pellet fragments from failed rods. In past research projects, computational models for these phenomena have been developed, implemented in an extended version of the FRAPTRAN-1.5 computer program and validated against results from relevant experiments on high-burnup PWR fuel. The models are of best-estimate nature, mechanistic, and deemed applicable to conditions also beyond those covered by their validation database, most importantly to the conditions simulated in this work. The models are used for analysing the thermal-mechanical behaviour of fifty fuel rods that are operated under normal conditions in the Ringhals 4 PWR until they are finally exposed to a LB LOCA at end of their final operating cycle. The rod average burnup and linear heat generation rate (LHGR) when the postulated LOCA occurs is in the range 49-63 $MWd(kgU)^{-1}$ and 2.6-19.2 kWm^{-1}, respectively, for the analysed rods.

The calculations show that fuel rods operating with an LHGR below 15 kWm^{-1} when the LOCA occurs experience negligible deformation, oxidation and damage during the postulated accident, and the aforementioned high-burnup phenomena are not manifested. For fuel rods operating with higher pre-LOCA power, the calculated cladding tube deformations are sufficient to cause local collapse of the fuel pellet column and subsequent axial relocation of the crumbled fuel. The analyses suggest that the axial relocation has a strong detrimental effect on the fuel rod behaviour, primarily through the local increase in fuel and cladding temperature that it brings about. This temperature increase, in turn, increases fuel pellet fine fragmentation and transient fission gas release, as well as cladding oxidation and embrittlement. In fact, the fuel fragment axial relocation induces a clear threshold effect for these phenomena, since the calculations show large differences between fuel rods that experience fuel relocation and those that do not. Cladding failure is calculated for four of the fifty rods. The failures cause moderate dispersal of fuel fragments, amounting to at most 8.5 % of the rod inventory.

The best-estimate fuel rod analyses are supplemented by parametric studies and sensitivity analyses to elucidate the impact of model parameters and modelling assumptions.

Sammanfattning

Föreliggande rapport beskriver en *in-silico* studie, i vilken det termomekaniska beteendet hos högutbrända UO_2-bränslestavar under en postulerad olycka med stort rörbrott och kylmedelsförlust (LB LOCA) i en tryckvattenreaktor (PWR) simuleras med bästa tillgängliga beräkningsmodeller. Studien syftar till att bedöma i vilken mån vissa högutbränningsfenomen, vilka observerats i experiment under icke-prototypiska förhållanden, kommer till uttryck i bränslestavar av modern design, då dessa vid slutet av sin livslängd utsätts för en typisk konstruktionsgrundande PWR LB LOCA.

De högutbränningsfenomen som beaktas är fin fragmentering av bränslekutsar, transient fissionsgasfrigörelse i kombination med begränsat axiellt gasflöde, axiell omfördelning av fragmenterat bränsle, samt utspridning av bränslefragment från skadade stavar. I tidigare forskningsprojekt har beräkningsmodeller för dessa fenomen utvecklats, implementerats i en utvidgad version av beräkningsprogrammet FRAPTRAN-1.5 och validerats mot resultat från relevanta experiment, utförda på PWR-bränsle med hög utbränning. Modellerna är av best-estimate karaktär, mekanistiska, och bedöms vara tillämpliga även för förhållanden som ej täcks av deras valideringsdatabas, i synnerhet de förhållanden som simuleras i detta arbete. Modellerna används för att analysera det termomekaniska beteendet hos femtio bränslestavar, vilka efter normal drift i Ringhals 4 utsätts för en LB LOCA vid slutet av deras sista driftscykel. De analyserade stavarnas medelutbränning och linjära medeleffekt (LHGR) är 49-63 $MWd(kgU)^{-1}$ respektive 2.6-19.2 kWm^{-1}, när den postulerade LOCA:n inträffar.

Beräkningarna visar att bränslestavar som körs med lägre LHGR än 15 kWm^{-1} när LOCA:n inträffar erfar försumbar deformation, oxidation och skadlig påverkan under den postulerade olyckan. Ej heller kommer ovan nämnda högutbränningsfenomen till uttryck. För bränslestavar med högre pre-LOCA effekt, är de beräknade kapslingsrörsdeformationerna tillräckliga för att orsaka lokal kollaps av bränslekutspelaren, följt av axiell omfördelning av det fragmenterade bränslet. Analyserna antyder att den axiella omfördelningen har en stark skadlig effekt på bränslestavbeteendet, huvudsakligen genom den lokala höjning av temperaturen hos bränsle och kapsling som den leder till. Temperaturhöjningen leder i sin tur till mer omfattande bränslekutsfragmentering och transient fissionsgasfrigörelse, liksom oxidation och försprödning av kapslingsrören. Den axiella omfördelningen av bränslefragment leder till en tydlig tröskeleffekt för dessa fenomen, då beräkningarna visar på stora skillnader mellan bränslestavar som uppvisar bränsleomfördelning och de som inte gör det. Kapslingsrörsskador beräknas för fyra av de femtio stavarna. Skadorna leder till begränsad utspridning av bränslefragment, som högst 8.5 % av stavens inneslutna bränslemängd.

Bränslestavanalyserna av best-estimate karaktär kompletteras med parameterstudier och känslighetsanalyser för att klarlägga inverkan av modellparametrar och modelleringsantaganden.

1. Introduction

1.1. Background

Loss-of-coolant accidents (LOCAs) in light water reactors (LWRs) may lead to overheating of the fuel rods, which in turn may lead to distension and rupture of the internally overpressurized cladding tubes that enclose the oxide fuel pellets. The temperature excursion may also cause loss of cladding ductility by high temperature oxidation of the material, leading to brittle failure when the cladding is finally re-wetted (quenched) by the emergency core cooling system. To maintain structural integrity of the fuel and to ensure that the reactor core remains coolable, the cladding temperature and oxidation should not transgress certain limits [1]. Specifically designed computer programs are used for confirming that these acceptance criteria are met for postulated accident scenarios, so called design basis accidents (DBAs). A widely used program for thermal-mechanical analysis of LWR fuel rods under accident conditions is FRAPTRAN [2], developed and maintained by the Pacific Northwest National Laboratory, USA.

A general conception is that fuel rods with low or moderate burnup are those that are most likely to be damaged under a typical LWR DBA LOCA, while high-burnup rods, due to their lower power, are unlikely to fail [3]. However, for the last two decades, this conception has been challenged by results from LOCA tests on high-burnup fuel. For example, separate effect tests have shown that long-term hydrogen uptake from cladding in-service waterside corrosion aggravates cladding embrittlement by high-temperature oxidation during LOCA [4, 5]. This hydrogen effect reduces the post-quench ductility for cladding tubes of high-burnup fuel rods. Moreover, in high-burnup fuel rods, high-temperature cladding oxidation under LOCA may occur not only from the waterside, but also from the cladding inside, by firm contact (bonding) with the oxide fuel pellets. In addition, integral and semi-integral LOCA simulation tests have shown that high-burnup fuel pellets may turn into very fine (< 0.1 mm) fragments during LOCA, and that this pulverization-like fragmentation is concomitant with rapid release of gaseous fission products [6-11]. These tests have also shown that the finely fragmented fuel easily relocates axially into parts of the fuel rod that balloon (distend) during LOCA. The relocation of fuel fragments increases the local heat load in the ballooning part of the rod, and the fine fragments are readily dispersed into the coolant, should the balloon rupture. These interconnected high-burnup phenomena are known under the acronym FFRD – Fuel fragmentation, relocation and dispersal [12-15]. They are generally not explicitly modelled in computer programs that are currently used for thermal-mechanical analysis of LWR fuel rod behaviour under LOCA.

Although the aforementioned LOCA simulation tests give evidence that fuel fine fragmentation and axial relocation of the fragments are aggravating phenomena in

high-burnup fuel rods, it should be recognized that many of the tests were deliberately designed to amplify the phenomena, and they are therefore not fully representative for conditions expected under LOCA in commercial LWRs [13-16]. The most important differences between the testing conditions and the conditions expected under typical DBA LOCA in light water reactors are:

- The burnup of the tested fuel is in many cases higher than today's typical discharge burnup of commercial LWR fuel;
- The tests are done on single rodlets, whose cladding tube distension is not limited by contact with neighbouring fuel rods, as it would be in a real fuel assembly. Moreover, most tests are conducted without mechanical constraints equivalent to those imposed by spacer grids in a fuel assembly;
- In most tests, the ratio of the gas plenum volume to the rod active length is an order of magnitude larger than in commercial LWR fuel designs. This is partly due to length restrictions for the test rodlets, but also because the plenum is usually connected with pressure transducers through fairly voluminous lines. Moreover, in the test rodlets, the plenum is closer to the hot ballooning part of the cladding than in a full-length fuel rod. Much of the cladding deformation in the tests is therefore driven by plenum gas that flows to the ballooning part;
- Tests are performed by heating the test rods from a low (~600 K) initial temperature, while the LWR LOCA initiates from a high fuel pellet centreline temperature, drops and equilibrates during the blowdown phase, and then rises again. This difference may affect the fuel pellet fragmentation behaviour;
- Out-of-reactor LOCA simulation tests on high-burnup fuel rods are carried out with external (furnace) heating. Cladding burst in externally heated fuel rods is claimed to occur at lower temperature than in internally heated rods [17];
- Axial gradients in test rodlet power and/or temperature are steeper than those expected under the high temperature phase of an LWR LOCA;
- Heating rates in the tests are generally lower than those expected for LWR LOCA, while the opposite is true for the peak temperature.

These differences accentuate fuel fine fragmentation and/or localized cladding deformation in the test rodlets, and thus, they contribute to the axial fuel relocation and the aggravating effects that it brings about. In conclusion, it may be expected that detrimental effects of FFRD may not be as severe in a typical DBA light water reactor LOCA as observed in many LOCA simulation tests.

1.2. Objective and scope

The work in this report aims to assess the importance of high-burnup phenomena for the fuel rod behaviour in a pressurized water reactor (PWR) large-break (LB) loss-of-coolant accident by use of state-of-the-art, mechanistically based, computational models. The high-burnup phenomena of interest are fuel pellet fine fragmentation, transient fission gas release in combination with restricted axial gas flow, axial relocation of fragmented fuel, and dispersal of fuel fragments from failed rods.

To this end, computer simulations with best-estimate models are carried out for altogether fifty high-burnup fuel rods, operated under normal conditions in the Ringhals 4 PWR, Sweden, until they are finally exposed to a large-break LOCA at end of their final operating cycle. The design and in-service operating conditions for the simulated fuel rods are realistic and represent fifty selected real-world fuel rods that were discharged in 2022 after cycle 39 in Ringhals 4. The calculated average burnup of the selected rods ranges from 49 to 63 MWd(kgU)$^{-1}$, while the peak pellet burnup is 53-69 MWd(kgU)$^{-1}$.

The transient thermal-mechanical boundary conditions for the analysed fuel rods are taken from an earlier RELAP5/MOD3 analysis of a postulated LB LOCA in Ringhals 4 [18]. The postulated scenario for the considered accident is deemed credible but conservatively bounding with regard both to the duration of the accident and the peak temperatures reached. The high-burnup phenomena that we set out to study are triggered, to various extent, with this accident scenario. To confirm that the selected LB LOCA scenario is conservative in terms of fuel rod thermal-mechanical boundary conditions, a less challenging accident scenario is considered in supplementary analyses of the same set of high-burnup fuel rods. This accident scenario, which is representative for a typical LB LOCA analysis with best-estimate plus uncertainty (BEPU) methodology, leads to relatively mild consequences that are insufficient for triggering the high-burnup fuel rod phenomena of interest in this report.

The presented fuel rod analyses are carried out with FRAPCON-QT-4.0P1 and FRAPTRAN-QT-1.5. The latter program is equipped with an extensive set of best-estimate models for the high-burnup phenomena to be analysed. These models have been developed, numerically implemented, and successfully validated against integral and semi-integral LOCA experiments on high-burnup LWR fuel in earlier research projects for the Swedish Radiation Safety Authority (SSM). Since the models are mechanistic in nature, they are deemed applicable to conditions beyond those covered by this experimental database, most importantly to the conditions simulated in this work.

1.3. Organization of the report

The report is structured as follows:

Section 2 of the report defines the accident scenario and the high-burnup fuel rods considered in the presented analyses. In addition, the applied software and computational models are described, together with key input and assumptions. More detailed information on these issues is provided in Appendices A-C.

Results of the fuel rod analyses are presented and discussed in section 3. Calculated results for the pre-LOCA fuel rod conditions, serving as initial conditions for the postulated LOCA, are first presented. This is followed by calculated results for the accident progression, and finally, for the post-LOCA fuel rod conditions.

Finally, section 4 is a summary of the most important results and conclusions from the work. Sensitivity analyses and parametric studies, intended to supplement the best-estimate calculations, are presented and discussed. Uncertainties and shortcomings of the presented analyses are identified, and suggestions are made for further work.

Since Appendices C and D contain confidential information, they are not included in the public version of the report.

2. Scope of analysis and applied methods

This work is an *in silico* study of the thermal-mechanical behaviour of high-burnup fuel rods under a PWR large-break LOCA. The behaviour of altogether fifty high-burnup fuel rods, operated for four reactor cycles in the Ringhals 4 (R4) PWR, is studied for a postulated accident scenario in the same reactor. The computer programs used for the analysis are defined in Fig. 1, where also key input data and data transfer between the programs are summarized.

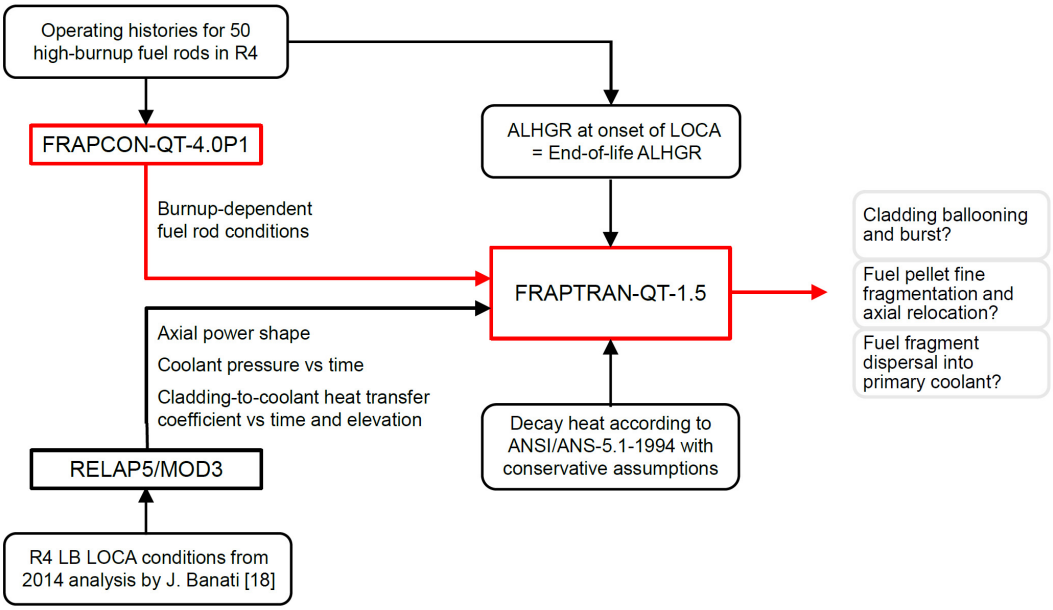

Fig. 1: Summary of software, data transfer and key input/output for the analysis. Boxes in red define the fuel rod analyses performed in the current part of the work (normal steady-state operating conditions, followed by end-of-life large break LOCA).

The work presented in this report is restricted to thermal-mechanical fuel rod analyses, which means that the RELAP5/MOD3 system analysis of a large-break LOCA in Ringhals 4, indicated in Fig. 1, is not covered here. However, the postulated accident scenario is summarized in section 2.1 below, and results from the RELAP5/MOD3 analysis that serve as thermal-mechanical boundary conditions to our fuel rod analyses are documented in Appendix A. Details of the RELAP5/MOD3 analysis are given in [18] and references therein.

Section 2.2 deals with steady-state thermal-mechanical fuel rod analyses, conducted with FRAPCON-QT-4.0P1, to establish the pre-LOCA conditions of fifty selected high-burnup fuel rods. The simulated operating histories for these rods represent those of real-world fuel rods, discharged after cycle 39 in Ringhals 4. In section 2.3, the transient thermal-mechanical fuel rod analyses of the postulated LOCA are outlined. These analyses were done with FRAPTRAN-QT-1.5, using

an extensive set of models that have been developed for analysis of high-burnup fuel behaviour under LOCA conditions in earlier research projects for SSM.

Both FRAPCON-QT-4.0P1 and FRAPTRAN-QT-1.5 are best-estimate computational tools, and the presented fuel rod analyses should be considered as best-estimate. When needed, the best-estimate analyses are supplemented with parametric studies to elucidate the impact of model parameters or modelling assumptions.

2.1. Postulated large-break LOCA scenario

The postulated accident scenario is a typical design basis large-break LOCA, occurring in the Ringhals 4 PWR, Sweden. This reactor is of three-loop Westinghouse design, constructed in the late 1970s, which has recently been upgraded to a thermal capacity of 3.3 GW [19]. The core consists of 157 fuel assemblies with a 17×17 rod lattice design.

In connection with the capacity upgrade, which was approved by the Swedish Radiation Safety Authority in 2018, SSM commissioned an independent analysis of large-break LOCA in the upgraded reactor. The analysis was performed with the RELAP5/MOD3 computer program at the Division of Nuclear Engineering, Chalmers University of Technology, Sweden. Results from this analysis are used as thermal-mechanical boundary conditions to the fuel rod analyses presented in this report. The postulated accident scenario, the RELAP5/MOD3 computational model and the results of the system analysis are described in [18, 20].

In summary, the consequences of a double-ended full cross-sectional (200 %) guillotine break in the cold leg of the coolant loop that contained the pressurizer was studied parametrically by varying the pre-LOCA thermo-hydraulic conditions in the primary system and the start-up time and capacity of emergency core cooling systems. In total, about 25 cases with sampled parameters were considered in this parametric study. Here, we will only consider the limiting case (#24) that resulted in the highest calculated peak cladding temperature (1238 K). This case is characterized by a significant delay (30.8 s) for delivery of water by the low- and high-head safety injection systems. The delay, which has a penalizing effect on fuel and cladding temperatures during the accident, is caused by an assumed loss of off-site power. Due to this assumption, the peak temperatures are also reached fairly late in the accident, during the refill phase, in contrast to accident scenarios where peak temperatures are reached during the initial blowdown phase. In view of fuel rod damage, the postulated scenario should be considered conservative, since it is challenging with regard both to the duration of the accident and the peak temperature reached. The reader is referred to [18] for further details on the assumed accident scenario, the applied RELAP5/MOD3 model, and the calculated results.

Appendix A contains results extracted from the limiting case in [18], which are here applied as transient fuel rod thermal-mechanical boundary conditions in the

fuel rod LOCA analyses. These boundary conditions comprise the fuel rod axial power distribution, the reactor coolant pressure and saturation temperature versus time, and the space-time evolution of cladding-to-coolant heat transfer coefficients; see Fig. 1.

2.2. Fuel rod pre-LOCA modelling

With the aim to study the consequences of a large-break LOCA to high-burnup fuel, we consider fifty fuel rods that have reached the end of their operating life when the postulated LOCA occurs. More precisely, the postulated LOCA is assumed to occur at the very end of cycle 39 in Ringhals 4.

2.2.1. Computational models

The pre-LOCA conditions of the selected fuel rods were established by modelling their operating life up to the LOCA with the FRAPCON-QT-4.0P1 computer program; see Fig. 1. This in-house version of FRAPCON-4.0P1 contains models for the behaviour of gaseous fission products in the fuel material [21] that are more elaborate than the models available in the standard version of the program [22]. In particular, the models calculate the space-time evolution of gas cavity properties (average cavity size, number density, gas content and pressure) in grain boundaries and the high-burnup structure (HBS) at the pellet rim. These gas cavity properties are essential for modelling fuel pellet fine fragmentation and transient fission gas release during the postulated LOCA [21]. Aside for the fission gas models, recommended default models and options were used in the calculations with FRAPCON-QT-4.0P1. In particular, the thin-shell mechanical model was used for the cladding tube, rather than the finite element based model.

The standard version of FRAPCON-4.0P1 is validated for modelling UO_2 fuel rods with an average burnup up to 62 MWd(kgU)$^{-1}$ [22], and our in-house models for fission gas behaviour in FRAPCON-QT-4.0P1 are validated against data from fuel with even higher burnup [21]. Hence, the fuel rods analysed in this work fall within the range of application for FRAPCON-QT-4.0P1; see section 2.2.2 below.

In calculations with both FRAPCON-QT-4.0P1 and FRAPTRAN-QT-1.5, the fuel rods were discretized axially into 36 equal-length axial segments. Radially, the fuel pellet stack was discretized into 50 nodes in temperature calculations and 100 equal-volume annuli in fission gas calculations. This radial discretization is significantly finer than normally used in calculations with FRAPCON and FRAPTRAN. It was used in order to spatially resolve fuel pellet fine fragmentation and transient fission gas release during the postulated LOCA.

The use of identical discretization in the two programs simplified transfer of data from FRAPCON-QT-4.0P1 to FRAPTRAN-QT-1.5. These burnup-dependent data comprise permanent deformations of fuel and cladding, fission gas distributions within the fuel pellet column and the rod free volume, fuel pellet local mi-

crostructural characteristics, burnup and content of fissile isotopes (important for the radial power distribution within the fuel pellets), and cladding state of water-side corrosion and hardening by fast neutron damage. Most of these calculated data are presented and discussed in section 3.1 of the report.

2.2.2. Fuel rod design and operating histories

A generic 17×17 fuel rod design, representing the fuel used in Ringhals 4 during the considered operating cycles, was assumed in the analyses with FRAPCON-QT-4.0P1. A summary of this design is given in Table 1, and further details are presented in Appendix C. A modern Zr-Sn-Nb type cladding material was assumed, which in our simulations with FRAPCON-QT-4.0P1 was represented by the program's existing models for Optimized ZIRLO™ [22].

Operating histories for the fifty analysed fuel rods were provided by Vattenfall Nuclear Fuel AB [23]. These operating histories are based on reactor core design data and represent fifty real fuel rods that were discharged after cycle 39 in Ringhals 4. The selected rods have end-of-life average burnups between 49 and 63 MWd(kgU)$^{-1}$ and their end-of-life rod average linear heat generation rate (ALHGR) covers a spectrum from 2.6 to 19.2 kWm^{-1}; see Fig. 2. These end-of-life burnups and ALHGRs define the fuel rod conditions at onset of the postulated LOCA. However, the axial power distribution in each fuel rod is assumed to change from its end-of-life steady state profile (modelled in FRAPCON-QT-4.0P1) to a more upper-peaked transient profile (modelled in FRAPTRAN-QT-1.5) during the postulated LOCA; see Appendix A. The power-versus-burnup spectrum covered by the selected fuel rods is shown in Fig. 3. More detailed information on the fuel rod operating histories is provided in Appendix C.

Table 1: Summary of generic fuel rod design considered in analyses.
Further details on the design are given in Appendix C.

Rod active length	[mm]	3658
Rod internal free volume	[cm^3]	19.19
Fuel rod-to-rod pitch in the assembly	[mm]	12.6
Helium fill gas pressure at room temperature	[MPa]	2.10
Fuel pellet material		Std UO_2
Fuel pellet density	[kgm^{-3}]	10 509
Fuel pellet diameter	[mm]	8.192
Cladding tube material		Zr-Sn-Nb
Cladding outer diameter	[mm]	9.500
Cladding inner diameter	[mm]	8.357

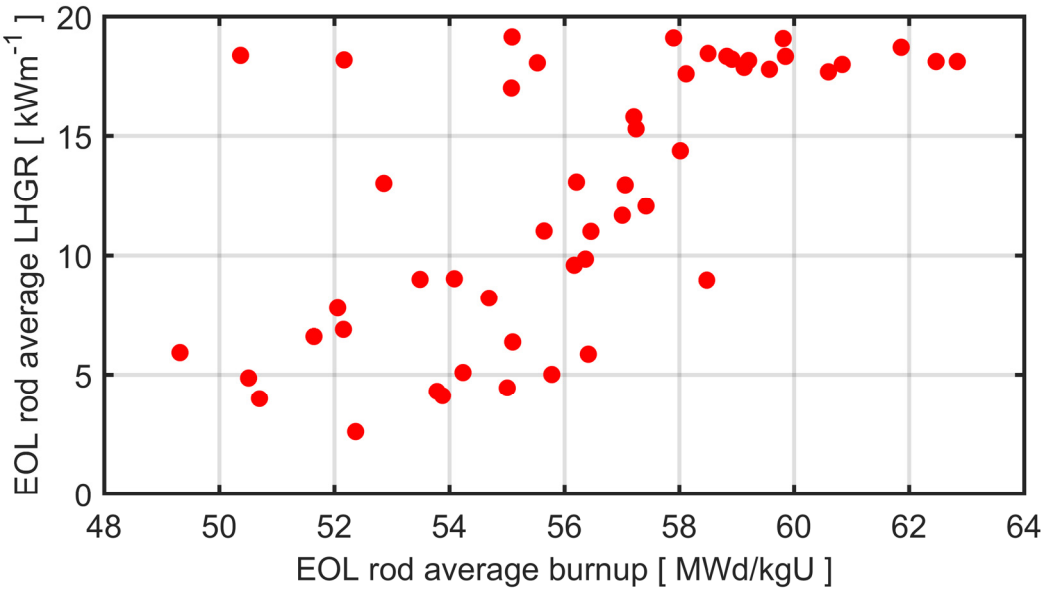

Fig. 2: End-of-life (EOL) rod average LHGR versus EOL rod average burnup for the fifty fuel rods considered in the analyses. Further details are given in Appendix C.

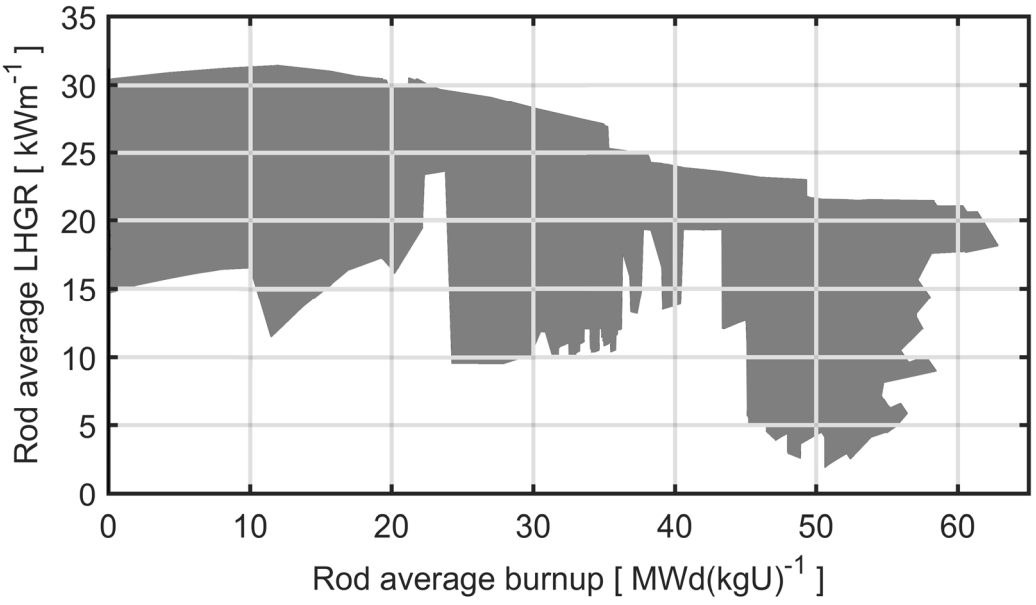

Fig. 3: Power-versus-burnup spectrum covered by the fifty fuel rods considered in the analyses. Power histories for individual fuel rods are given in Appendix C.

2.3. Fuel rod LOCA modelling

2.3.1. Computational models

The fuel rod thermal-mechanical behaviour under the postulated large-break LOCA was modelled with FRAPTRAN-QT-1.5, an extended in-house version of FRAPTRAN-1.5 that is significantly different from the standard version [24]. Firstly, our extended version of the program contains the same set of models for calculating the space-time evolution of fuel pellet microstructure and fission gas distribution as implemented in FRAPCON-QT-4.0P1 [21]. The fact that the same models are used in both programs makes it easy to simulate a postulated transient that follows after long-term operation: data relating to fuel microstructure and fission gas distribution are transferred from FRAPCON-QT-4.0P1 to FRAPTRAN-QT-1.5 via a specific interface file. Secondly, FRAPTRAN-QT-1.5 contains models for axial relocation of fuel pellet fragments and the re-distribution of heat load that this relocation entails [25]. Thirdly, it comprises a set of models that treat cladding high temperature metal-water reactions, solid-solid phase transformation, creep and failure in a unified fashion [26, 27]. Fourthly, an advanced model for axial gas flow and mixing in the pellet-cladding gap has recently been implemented [28]. An important parameter in this model is the axial transmissivity of gas, which depends on the local crack density in the fuel pellets and on the local width of the pellet-cladding gap; see section B.1 of Appendix B for a summary of the expressions used for estimating the transmissivity for axial gas flow. Finally, a number of errors and shortcomings observed in the standard version of FRAPTRAN-1.5 have been fixed [29].

All calculations were done with a slightly modified version of the finite element based mechanical solution module [30] in FRAPTRAN-QT-1.5. The modifications include use of the aforementioned set of cladding high-temperature material models [26, 27] and a rod-to-rod contact model that includes friction. The latter is important for restricting axial deformation of the cladding tube, once it has ballooned to an extent that it comes in contact with neighbouring fuel rods.

A stress-based burst criterion was used for predicting high-temperature rupture of the cladding tube. The criterion, which is briefly described in section B.2 of Appendix B, has been calibrated against an extensive database of cladding burst tests and LOCA simulation tests, together with the high-temperature cladding creep model in FRAPTRAN-QT-1.5 [31]. The burst criterion and the creep model are applicable to Zircaloy and Zr-Sn-Nb type cladding.

From the time of cladding rupture, outflow of gas from the failed rod was calculated by use of a model for isentropic flow of a calorically perfect gas, which considers the area of the cladding breach when calculating the outflow rate [28]. The breach area is calculated by use of a best-estimate empirical model, fitted to an extensive data base [32]. Ingress of steam into the failed rod is also handled by

this model. Although the model clearly suggests that steam enters the failed rod only at the final cooldown phase of the LOCA, unrestricted high-temperature steam oxidation of the cladding inner surface within a distance of 3 inches (75 mm) from the cladding breach was in all analyses assumed to start immediately after cladding rupture. This conservative assumption was made for consistency with the standard version of FRAPTRAN-1.5 [24]. Cladding high-temperature metal-water reactions were modelled by use of the Cathcart-Pawel correlations for total oxygen uptake (weight gain) and oxide layer growth [33].

The model parameters used for the fuel axial relocation model in FRAPTRAN-QT-1.5 were those used in earlier work [25, 34-36]; see Table 2. However, the submodel used for calculating the fuel fragment packing fraction was slightly modified with regard to the original Westman model described in [25, 37]. These modifications are described in section B.3, Appendix B. Also parameters in the models for the space-time evolution of fuel pellet microstructure and fission gas distribution were identical to those used in earlier work [21], but the applied value for the UO_2 grain boundary fracture energy, $\mathcal{G}_{gb}$, was reduced to 2.5×10^{-3} Jm^{-2} and a temperature dependence for the fracture strength of the pellet high burnup structure was introduced. More precisely, the fracture strength was calculated through $\sigma_{hbs}^{cr} = 3\times10^{7}(1 - 5.56\times10^{-4}T_k)$, where T_k is the local temperature in kelvin and σ_{hbs}^{cr} is in Pa. These micro-scale strength parameters have been determined by calibrating the model for fuel fine fragmentation against recent Studsvik LOCA simulation tests [35, 36].

Table 2: Applied parameters in the FRAPTRAN-QT-1.5 fuel axial relocation model [25].

Model parameter		Value
Packing fraction for regions with large fuel fragments only, ϕ^{L}	[-]	0.69
Packing fraction for regions with small fuel fragments only, ϕ^{S}	[-]	0.72
Characteristic size of fuel fragments, created by pulverization, l_p	[mm]	0.10
Residual fraction of fuel mass, remaining in emptied regions of the cladding tube because of fuel-cladding bonding, x^r	[-]	0.01
Threshold pellet-cladding radial gap for fuel pellet fragment detachment and axial relocation, g^{th}	[μm]	200
Residual pellet-cladding radial gap in regions with crumbled fuel, g^r	[μm]	5.0

As already mentioned, the fuel rod spatial discretization used in calculations with FRAPTRAN-QT-1.5 was identical to the one used in FRAPCON-QT-4.0P1 for simulating the steady-state pre-LOCA operating histories. The time step length was set adaptively in FRAPTRAN-QT-1.5, according to recommended criteria, to ensure stability and accuracy of the numerical solution. A maximum time step length of 1 ms was enforced. The typical execution time for a single fuel rod LOCA analysis with FRAPTRAN-QT-1.5 was about 30 minutes on a mid-range Linux workstation.

2.3.2. Decay heat and thermal-mechanical boundary conditions

The fuel rod power during the postulated LOCA was calculated from the rod power at onset of the accident through a decay heat curve that is based on the 1994 version of the ANSI/ANS-5.1 standard [38]. In addition, a constant, upper-peaked axial power distribution was postulated for all analysed fuel rods; see Fig. 29 in Appendix A.

The applied decay heat curve is shown in Fig. 4. The curve is based on the ANSI/ANS-51-1994 standard [38]. In its original form, this standard does not define a simple curve for the decay heat, but there are recommendations [39] on how to make simplifying and reasonably conservative assumptions regarding e.g. pre-LOCA operating time, fissioning isotopes, neutron capture, actinides, uncertainties, etc., in order to get a simple curve that fits the requirements in Appendix K to U.S. 10 CFR part 50 [40]. Details regarding these assumptions are described in [39], together with comparisons of the resulting decay curve with results from alternative methods.

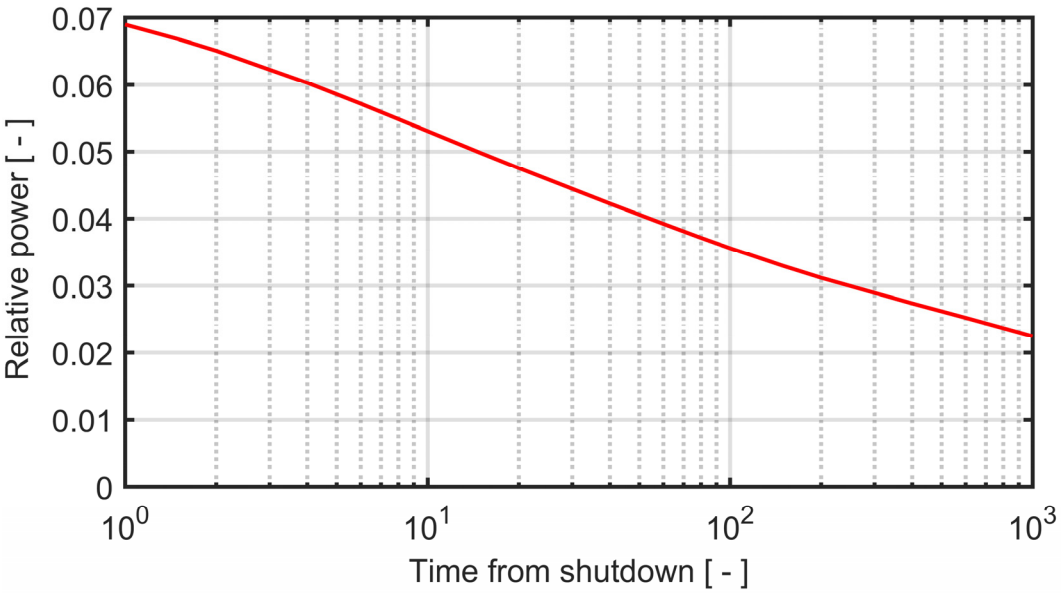

Fig. 4: Decay heat curve applied in the LOCA fuel rod analyses.

The thermal-mechanical boundary conditions applied to the fuel rods during LOCA comprise coolant pressure and temperature, and cladding-to-coolant heat transfer coefficients. These boundary conditions were extracted from the aforementioned RELAP5/MOD3 analysis of large-break LOCA in Ringhals 4 [18]. The boundary conditions are described in Appendix A, together with the methods used for extracting them from results reported in [18].

3. Results and discussion

Calculated results are presented and discussed below as follows: Section 3.1 deals with the pre-LOCA fuel rod conditions, calculated by use of FRAPCON-QT-4.0P1. The calculated fuel rod behaviour during the postulated accident is presented in section 3.2, whereas section 3.3 deals with the calculated post-LOCA fuel rod conditions.

3.1. Pre-LOCA fuel rod conditions

3.1.1. Fuel pellet burnup and microstructure

End-of-life axial distributions of fuel burnup, calculated with FRAPCON-QT-4.0P1, are shown in Fig. 5 for the fifty considered fuel rods. It is clear that the burnup distributions are fairly similar. The calculated peak pellet burnup is in the range from 53 to 69 MWd(kgU)$^{-1}$, and the peak is at z = 3.0 m for all rods.

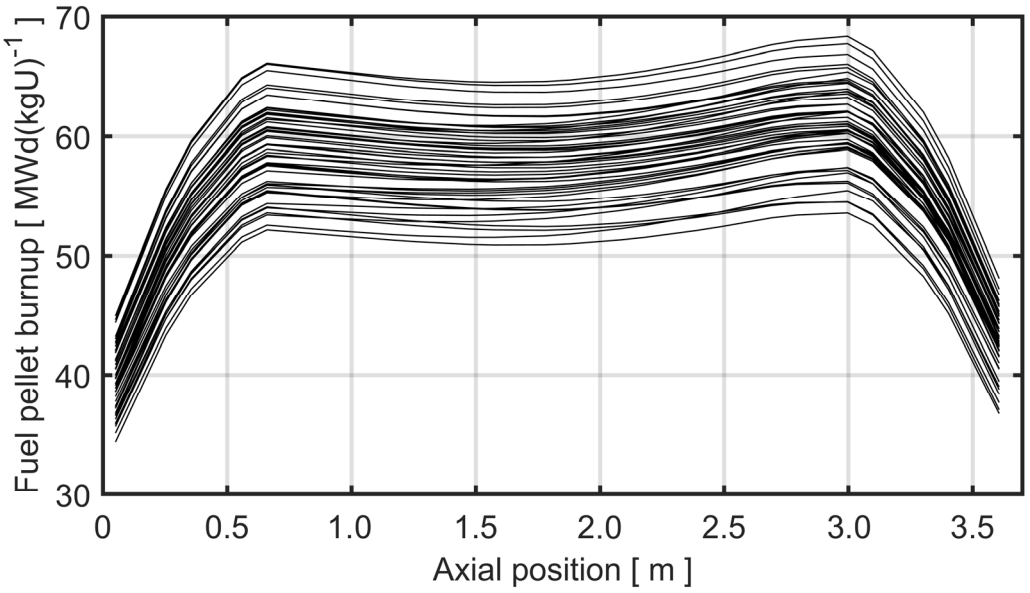

Fig. 5: Calculated end-of-life burnup distributions for the fifty fuel rods.

With regard to local burnup at the fuel pellet surface, the calculated (rim zone) maximum value over all fuel rods is 142 MWd(kgU)$^{-1}$. About 5-6 vol% of this particular fuel pellet had experienced high-burnup restructuring (rim zone formation), according to our calculations. Partial restructuring of the fuel material was calculated to a depth of about 0.2 mm from the pellet surface; see section 3.3.2 for more information on calculated rim zone properties.

3.1.2. Cladding corrosion

The calculated cladding waterside corrosion for the fifty analysed fuel rods is presented in Fig. 6. The calculated outer surface oxide layer thickness (left panel) and cladding metal layer hydrogen concentration (right panel) are plotted versus axial position along the fuel rods. Since the cladding corrosion models in FRAPCON are formulated with a linear relationship between oxide growth and hydrogen pick-up [22], the axial distributions for these two properties in a particular fuel rod are identical.

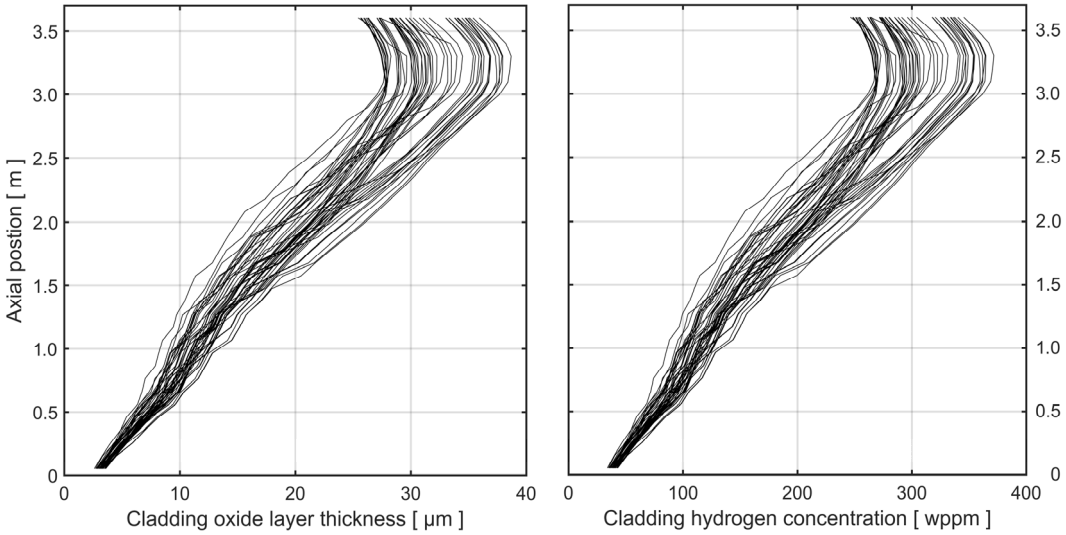

Fig. 6: Calculated cladding outer surface oxide layer thickness (left) and cladding metal layer hydrogen concentration (right).

Among the fuel rods, the calculated peak oxide layer thickness ranges from 27 to 38 μm, and the peak hydrogen concentration falls between 270 and 375 wppm. For all rods, the most corroded part is 3.2-3.3 m from the bottom of the fuel rod.

3.1.3. Fuel fission gas release and rod internal gas pressure

The left panel of Fig. 7 shows that the calculated end-of-life rod average fuel fission gas release ranges from about 1 to 5 % for the analysed rods. Moreover, the gas release is correlated to the lifetime rod average LHGR, although the correlation over the fairly narrow power range (17-25 kWm^{-1}) is weak. This is expected, since thermally activated (diffusion controlled) fission gas release is strongly affected by short periods at higher-than-average power and temperature. In addition, the axial distributions of power and temperature along the rod are important to the fuel fission gas release: Fig. 7 shows only rod average properties.

From the right panel of Fig. 7, it is clear that the calculated end-of-life rod internal gas pressure at cold (zero power, room temperature) conditions is increased by the

released fission gas. More precisely, the cold gas pressure typically increases by about 30 % for a fission gas release of 5 % at the considered fuel burnups.

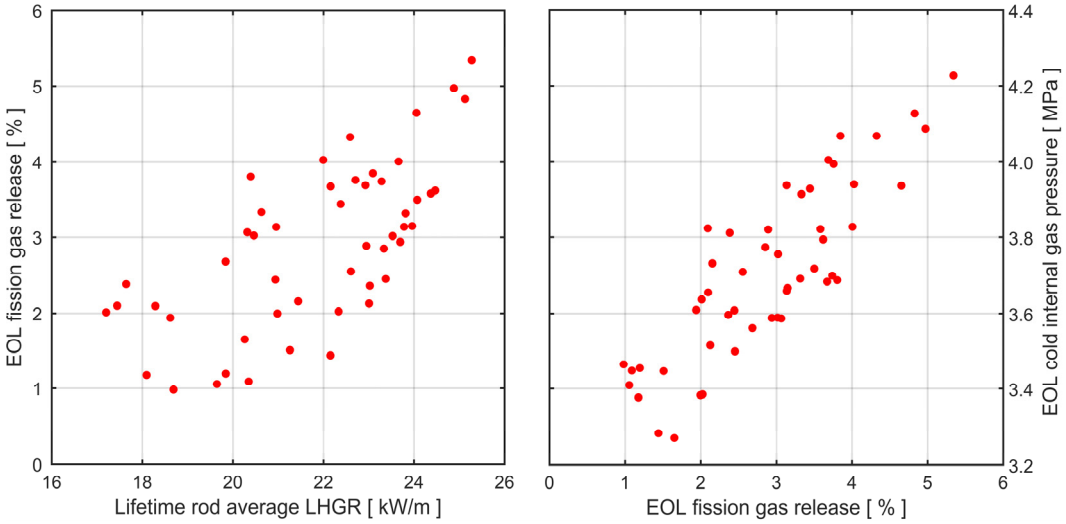

Fig. 7: Calculated end-of-life rod average fuel fission gas release versus lifetime rod average LHGR (left) and end-of-life rod internal gas pressure at zero-power room temperature conditions versus rod average fission gas release (right).

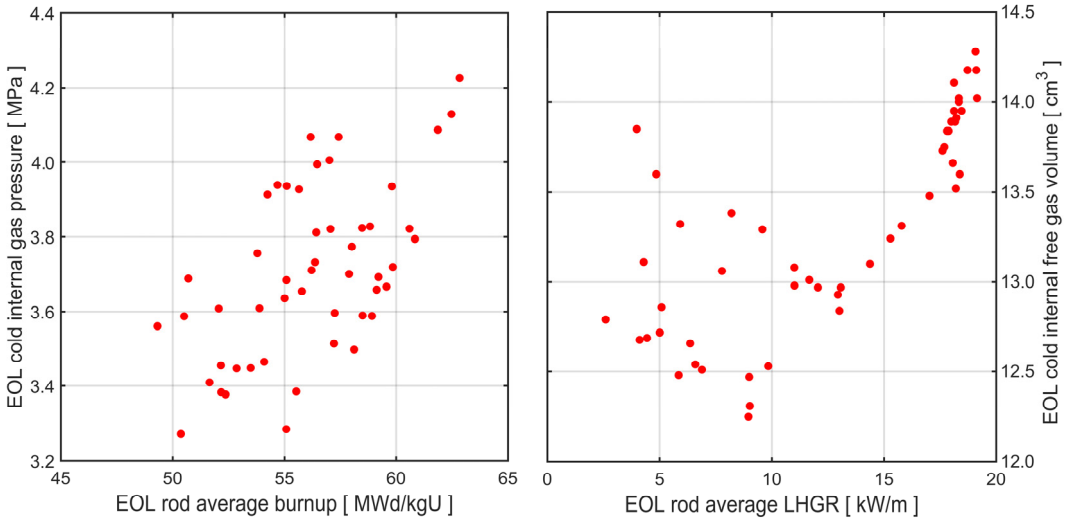

Fig. 8: Calculated fuel rod internal gas pressure at cold conditions versus rod average burnup (left) and rod internal free gas volume at cold conditions versus rod average LHGR (right). All properties are evaluated at end of the fuel rod's operating life.

The left panel of Fig. 8 shows the calculated end-of-life fuel rod internal gas pressure at cold conditions, plotted versus EOL rod average burnup. There is a clear trend of increasing gas pressure with burnup, but the spread is large. Along with the fuel fission gas release, shown in Fig. 7, the gas pressure depends also on the rod internal free gas volume. This parameter, evaluated at cold end-of-life condi-

tions, is plotted versus end-of-life rod average LHGR in the right panel of Fig. 8. For rods with an EOL average LHGR above 13-14 kWm^{-1}, the cold internal free volume is clearly correlated to the end-of-life fuel rod power. The reason is that much of the cold internal free volume in these high-power rods is created by gap opening from a firm pellet-cladding contact state when the fairly high power is brought to zero: the higher power at end-of-life, the wider and more voluminous will be the gap when the power is reduced to zero. This trend is clearly seen for the high-power rods in the right panel of Fig. 8.

Finally, the end-of-life rod internal gas pressure, calculated at hot (pre-LOCA) conditions with FRAPCON-QT-4.0P1, is shown in Fig. 9. Clearly, the calculated internal gas pressure at hot conditions correlates with both LHGR and fission gas release: the five rods with highest calculated pre-LOCA pressure (>10.5 MPa) are characterized by a combination of high end-of-life power and fuel fission gas release.

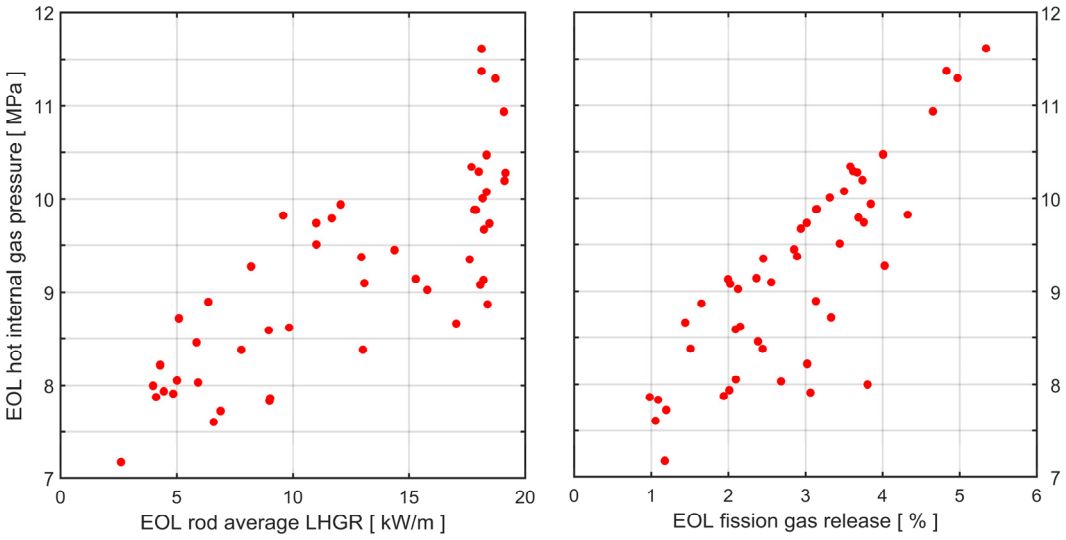

Fig. 9: Calculated fuel rod internal gas pressure at hot (pre-LOCA) conditions versus rod average LHGR (left) and rod average fission gas release (right). All properties are evaluated at end of the fuel rod's operating life.

3.2. LOCA fuel rod conditions

3.2.1. Cladding temperature

The peak cladding temperature, calculated versus time for each of the fifty fuel rods, is shown in Fig. 10. For each fuel rod, the peak value in each plotted time step is taken with respect to axial position. This peak temperature position changes over time, partly because of changes in local cladding-to-coolant heat transfer, partly because of fuel axial relocation. Fuel axial relocation, to various degrees, is

calculated for 22 of the fuel rods: the results for these rods are marked with red colour in Fig. 10.

Two effects of the fuel relocation can be observed in the calculated temperatures: i) the local heat load is increased in the lower part of the fuel rod's ballooned region, where the relocated fuel fragments accumulate; ii) the axial position of peak cladding temperature is moved downward to this part of the rod; see Fig. 13 below.

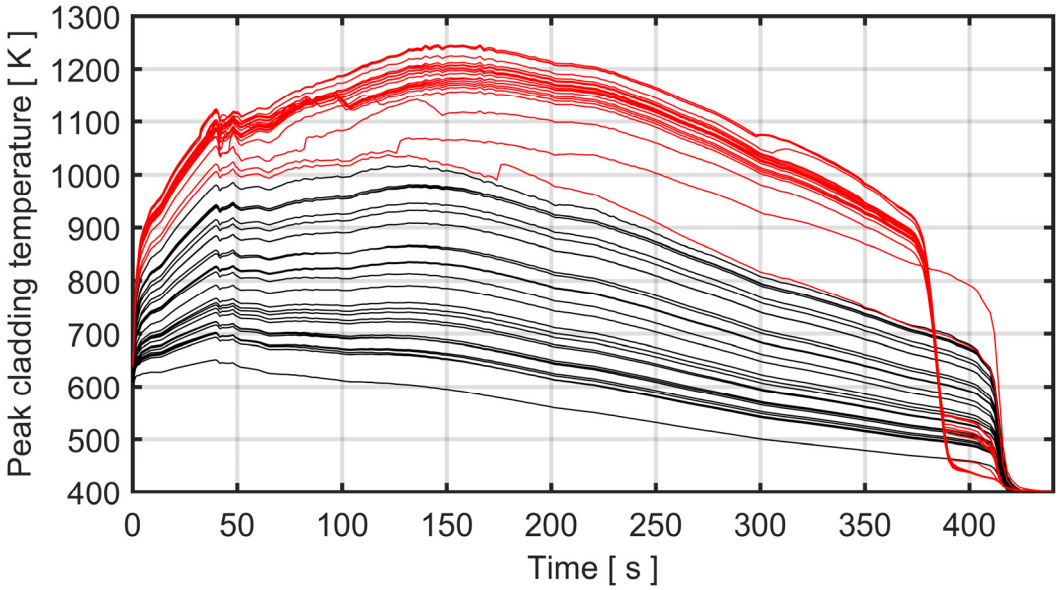

Fig. 10: Peak cladding temperature, calculated versus time, for each of the fifty fuel rods. Red curves indicate fuel rods, for which cladding ballooning and axial relocation of fuel fragments are calculated.

In order to investigate the impact of fuel axial relocation on cladding temperature, the 22 cases, for which relocation was calculated to occur, were simulated with the fuel relocation model deactivated in FRAPTRAN-QT-1.5 [25]. The results of this parametric study are shown in Fig. 11 and Fig. 12. The calculated increase in peak cladding temperature, caused by the relocation, ranges from about 30 to 300 K among the 22 fuel rods. The magnitude depends on how much fuel has been axially relocated in the rod; see section 3.3.1. Moreover, it is clear from Fig. 12 that the calculated temperature boost from relocation reaches its maximum fairly late in the accident, beyond 300 s. This is not surprising, since the radial conduction of heat from the crumbled fuel in the balloon is much slower than that from the fuel pellet column in its original form [25]. It is also interesting to note from Fig. 12 that the peak cladding temperature from 380 to 420 s is in most of the considered fuel rods actually *lowered* by the relocation. The reason is that the quench front at this time reaches the upper part of the balloon, which is also the position of peak cladding temperature. Since the axial relocation has emptied this part of the cladding tube, the local cladding temperature is lower than for a hypothetical case without relocation. Further (secondary) effects of fuel relocation are discussed in section 4.2.2.

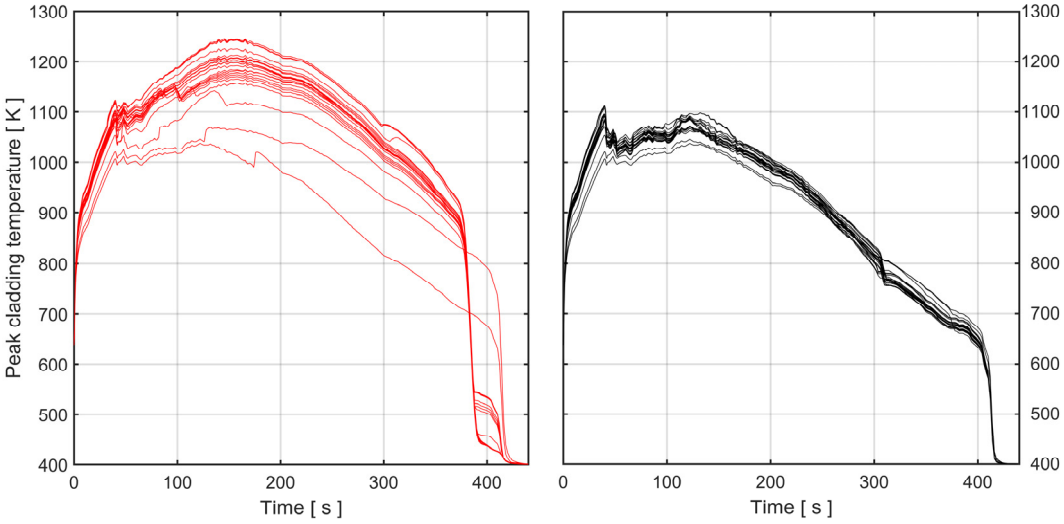

Fig. 11: Peak cladding temperature calculated in those 22 fuel rods that experience various degrees of fuel axial relocation (left), in comparison with calculations for the same fuel rods with the axial relocation model deactivated (right). See also section 3.3.1.

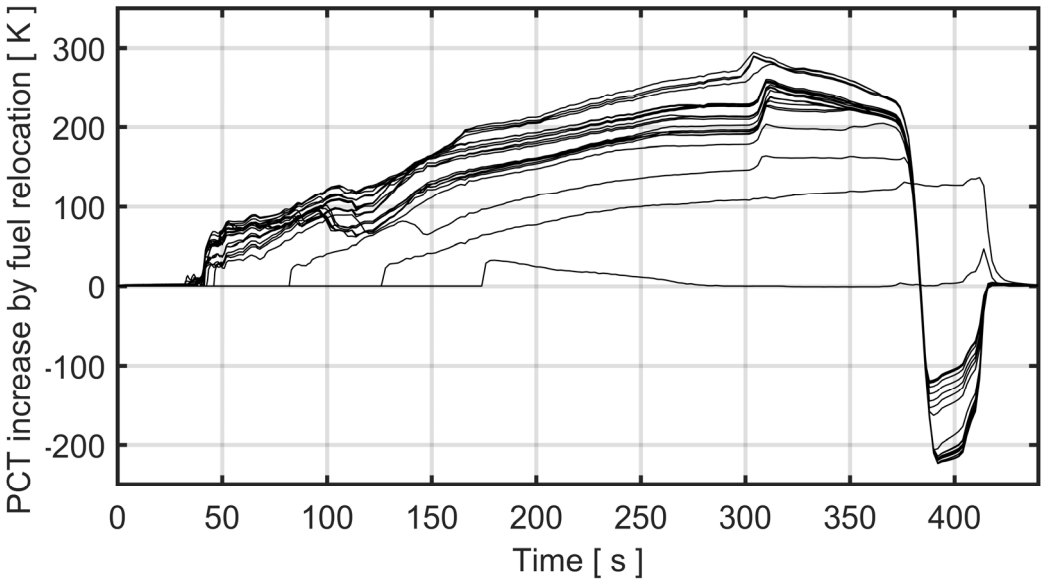

Fig. 12: Increase in peak cladding temperature by fuel axial relocation, calculated for the 22 fuel rods that experience various degrees of relocation.

The calculated peak cladding temperatures reached in the fuel rods follow a nearly linear relationship with the rod average LHGR at onset of the postulated LOCA. This is shown in the left panel of Fig. 13. The same figure also reveals that fuel axial relocation is calculated only for fuel rods with pre-LOCA average LHGR exceeding 15 kWm^{-1}. The reason is that very limited cladding distension (ballooning) is calculated for fuel rods with lower initial power. The right panel of Fig. 13 shows the calculated peak cladding temperature reached in a given axial position

over time. Cases with significant fuel axial relocation generally reach peak fuel and cladding temperatures at somewhat lower positions (~2.6 m) than cases without calculated relocation (~3.0 m). For the latter cases, the calculated position of peak fuel and cladding temperature coincides with the fuel rod peak power position; compare with Fig. 29 in Appendix A.

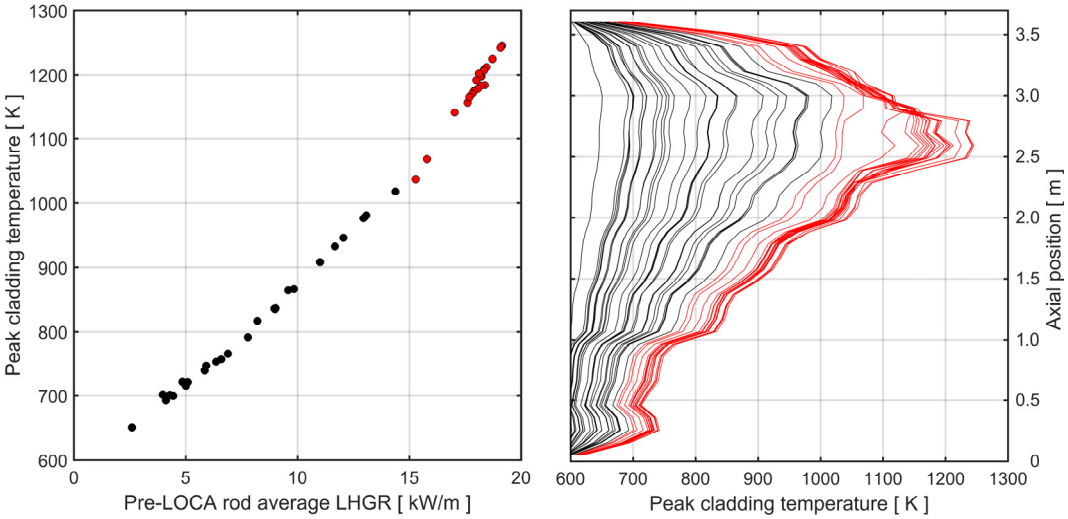

Fig. 13: Calculated peak (maximum over space and time) cladding temperature versus pre-LOCA rod average LHGR (left) and peak (maximum over time) cladding temperature versus axial position (right). Red colour indicates fuel rods, for which cladding ballooning and axial relocation of fuel fragments are calculated.

3.2.2. Rod internal overpressure

The left panel of Fig. 14 shows the calculated maximum rod internal overpressure over space and time for each of the fifty fuel rods, whereas the right panel shows the calculated overpressure in the ballooning part of the rod versus time. By comparing the two panels, it is clear that the overall peak internal overpressure is generally reached away from the ballooning part. The left panel of Fig. 14 shows that the overall peak internal overpressure is weakly correlated to the pre-LOCA rod average LHGR. This is consistent with the calculated trend for the hot pre-LOCA internal gas pressure, shown in the left panel of Fig. 9. In fact, by comparing the left panels of Fig. 9 and Fig. 14, it is clear that the overall peak rod internal overpressure correlates strongly with the hot pre-LOCA gas pressure.

The right panel of Fig. 14 reveals that the calculated peak overpressure in the ballooning part of the fuel rod is reached 20-25 s into the accident. By comparing the results for rods with and without fuel axial relocation, it is clear that the peak overpressure is reached somewhat earlier in rods that experience significant cladding ballooning and fuel relocation. These rods also exhibit a significant pressure drop after the peak, resulting from the increased free gas volume created by the balloon. Moreover, transient fission gas release is calculated to occur in these

high-power rods. This gas release shows up as bumps on the calculated overpressure curves in Fig. 14, typically in the time interval from 40 to 140 s. Transient fission gas release is further discussed in section 3.3.2.

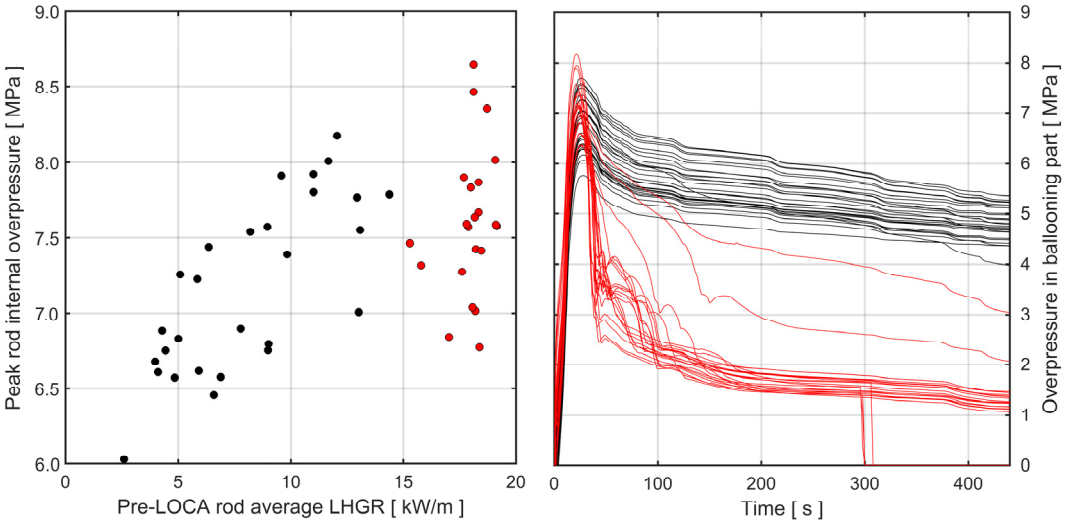

Fig. 14: Calculated maximum over space and time of rod internal overpressure (left) and overpressure versus time in ballooning part of the rod (right). Red markers and lines indicate fuel rods, for which cladding ballooning and axial relocation of fuel fragments are calculated

3.2.3. Cladding failure

Cladding failure by high-temperature rupture is in our analyses with FRAPTRAN-QT-1.5 predicted by use of a stress-based failure criterion, which is described in section B.2, Appendix B. Accordingly, cladding high-temperature rupture is assumed to occur if the ratio $\sigma_{\theta\theta}/\sigma_b$ (current cladding hoop stress / current predicted burst stress) reaches unity in any part of the cladding tube. In the following, we consider a cladding "damage index", defined as the ratio $\sigma_{\theta\theta}/\sigma_b$, expressed in percent. The damage index defines the relative risk for cladding failure, where 100 % corresponds to failure. It evolves with both space and time, as the cladding hoop stress, temperature and metal layer oxygen content changes; see section B.2 in Appendix B.

The left panel of Fig. 15 shows the calculated peak damage index, as a maximum over both space and time, for each fuel rod. Clearly, the peak damage index increases exponentially with increasing pre-LOCA LHGR. The calculated risk for cladding failure is low (< 30 %) for pre-LOCA ALHGR less than 15 kWm^{-1}, which is the calculated threshold for cladding ballooning and fuel axial relocation in the postulated accident scenario.

Four of the fifty fuel rods are calculated to fail during the postulated LOCA. These are the four rods with the highest pre-LOCA rod average LHGR in the

population. More precisely, their LHGR ranged from 18.7 to 19.2 kWm^{-1}, and their calculated pre-LOCA conditions are summarized in Table 3.

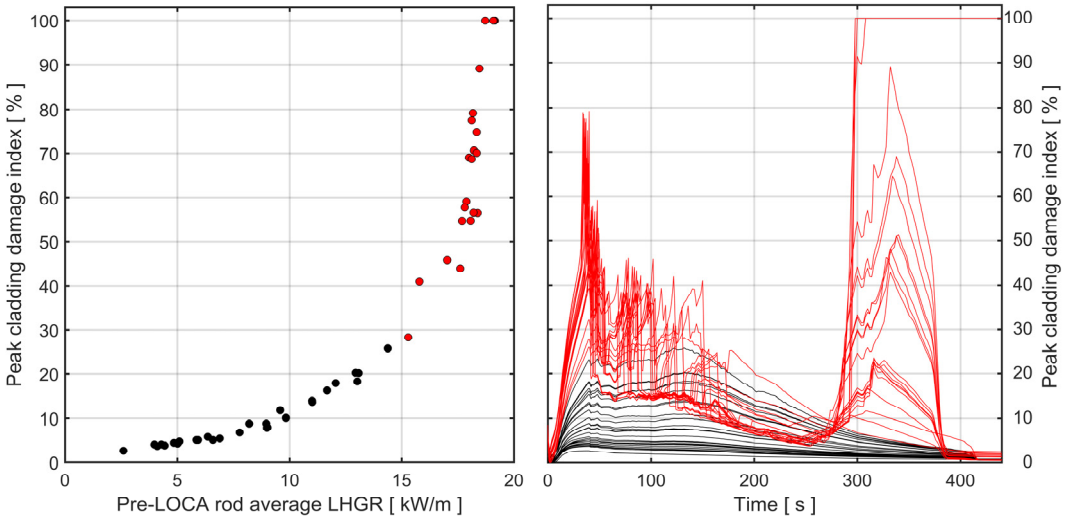

Fig. 15: Maximum cladding damage index over space and time versus fuel rod pre-LOCA ALHGR (left) and maximum damage index over space versus time for each rod (right). Fuel rods that experience cladding ballooning and fuel axial relocation are marked in red.

Table 3: Calculated pre-LOCA conditions for the four rods that are calculated to fail. Burnup, LHGR and fission gas release (FGR) are rod average values. Rod internal gas pressure (RIP) refers to hot pre-LOCA conditions.

Rod ID	Burnup [$MWd(kgU)^{-1}$]	LHGR [kWm^{-1}]	FGR [%]	RIP [MPa]
18	55.09	19.15	3.67	10.28
33	57.90	19.11	3.74	10.20
43	59.81	19.08	4.65	10.94
47	61.86	18.72	4.97	11.30

The calculated failure position is at z = 2.5 m for all four rods, and they are all calculated to fail late in the postulated accident, at t ~300 s. This somewhat unexpected result is clear from the right panel of Fig. 15, which shows the peak (maximum over space) cladding damage index, calculated versus time for each fuel rod. From this plot, it can be seen that all fuel rods that experience cladding ballooning and fuel axial relocation (red lines) have a late, secondary, peak for the calculated damage index. For these rods, the calculated damage index starts to increase from low (< 10 %) values at t ~250 s. Unless the rod is calculated to fail at t ~300 s, the damage index reaches a second peak, typically 320-340 s into the accident. At this time, the fuel rod has been cooled down by about 200 K from its peak value; compare with Fig. 10.

To understand the late failures, we consider the evolution of pertinent parameters, evaluated at the calculated failure position of rod #18, which is the rod with highest pre-LOCA ALHGR (19.15 kWm^{-1}) in our analysis. The left axis of Fig. 16 refers to the calculated cladding hoop and burst stress, as well as the damage index. The right axis of the figure refers to calculated cladding temperature and excess oxygen concentration in the cladding metal layer. These are the properties that determine the predicted cladding burst stress; see section B.2, Appendix B.

Evidently, the cladding hoop stress reaches a peak of 55 MPa about 20-25 s into the accident. At this time, the cladding is loaded only by the internal and external pressures, and the peak for $\sigma_{\theta\theta}$ therefore coincides in time with that for the internal overpressure; compare with the right panel of Fig. 14. The cladding tube distends by creep as a consequence of high temperature and internal overpressure, until it comes into contact with neighbouring fuel rods. In the finite-element based mechanical module that we use in FRAPTRAN-QT-1.5 [30], rod-to-rod contact is modelled by use of contact elements, assuming that neighbouring fuel rods distend just as much as the rod being analysed (mirrored boundary conditions). As a result of rod-to-rod contact forces, the calculated hoop stress first drops rapidly at t ~45 s and then slowly turns negative (compressive). At the same time, high-temperature metal-water reactions lead to a continuous increase of the cladding metal oxygen concentration, x_M, which embrittles the cladding significantly. More precisely, at t = 300 s, our calculations suggest that the oxygen-induced embrittlement has reduced the cladding burst stress to only 2.2 % of its pre-LOCA value at comparable temperature; see section B.2 of Appendix B.

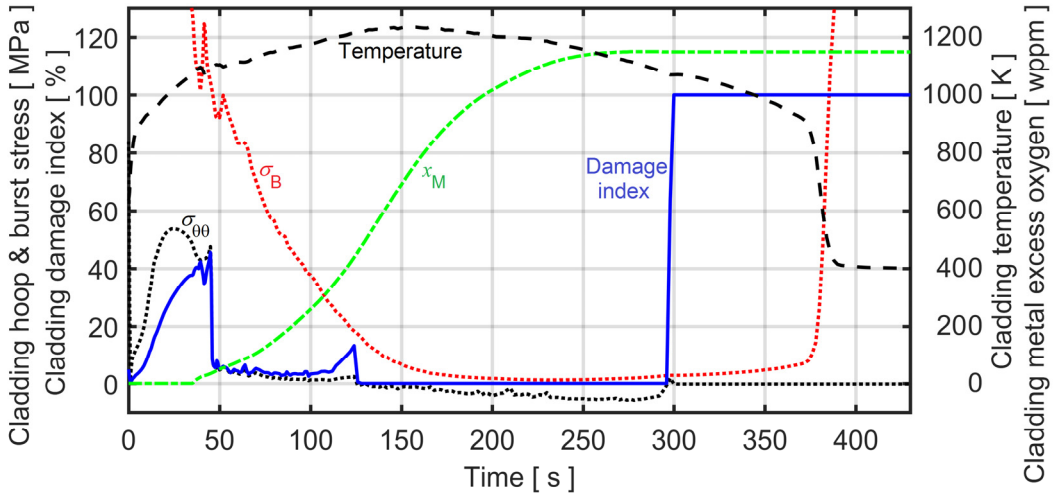

Fig. 16: Calculated evolution of pertinent parameters at the cladding failure position for fuel rod #18.

Finally, when the cladding temperature decreases, the cladding tube contracts and the rod-to-rod contact forces are relaxed. As a result of the relaxed contact forces during cooldown, the cladding hoop stress again turns positive (tensile). At t = 298.8 s, the calculated hoop stress exceeds the predicted burst stress (2.9 MPa)

and the cladding fails. The calculated cladding radial average temperature at failure is 1070 K and the cladding metal excess oxygen concentration is 1150 wppm. The example in Fig. 16 is for one of the failed rods, but similar sequences of events are calculated also for the other three rods that are predicted to fail.

3.2.4. Fuel fragment dispersal

As shown in section 3.2.3, the calculated failures occur late in the accident, at a time when the cladding material is oxidized and embrittled. The resulting cladding breaches are therefore small and crack-like, which means that only small fuel fragments may pass through the breach and be dispersed into the coolant.

An upper-bound estimate for the amount of dispersed fuel can be obtained by assuming that all fuel pellet fragments that are i) located above the cladding breach, ii) free to axially relocate downward to the breach position, iii) small enough to pass through the crack-like breach, are ejected into the coolant. Fuel fragments below the cladding breach are assumed to remain within the cladding tube, irrespective of their size. These assumptions must be considered as very conservative, since large, relocatable but non-dispersible, fragments are likely to hinder downward relocation and ejection of fine fragments. Nevertheless, Table 4 shows the estimated cladding breach dimensions for the failed fuel rods, together with the upper-bound estimates for the mass of relocatable and dispersible fuel fragments in each rod. Here, relocatable mass is the total mass of fuel fragments that are free to move downward to the cladding breach position (calculated by the axial relocation model), whereas dispersible mass refers to those fragments that are relocatable and small enough to pass through the cladding breach (calculated by the axial relocation model in combination with the model for fine fuel fragmentation).

Table 4: Calculated dimensions of the cladding breach and amounts of relocatable and dispersible fuel fragments in the failed rods. The dispersible fuel is an upper estimate for the amount of fuel that can be ejected from each failed rod; see the running text.

		Failed fuel rod			
Parameter		**18**	**33**	**43**	**47**
Rod overpressure at time of failure	[MPa]	1.40	1.43	1.56	1.67
Cladding temperature at time of failure	[K]	1070	1072	1071	1038
Cladding breach tangential width	[mm]	1.00	1.04	1.19	1.30
Cladding breach axial length	[mm]	7.26	7.40	7.90	8.25
Relocatable fuel mass	[g]	357	357	357	358
Dispersible fuel mass	[g]	168	172	168	165
Dispersible fraction of total inventory	[%]	8.3	8.5	8.3	8.1
- " - from empirical 'model A' in [13]	[%]	4.1	6.8	9.5	10.9

The cladding breach dimensions in Table 4 are best-estimate values, calculated from the rod internal overpressure at time of cladding failure through the empirical correlation presented in [32]. We recall from our assessment of experimental data in [32] that there is a significant variability in cladding rupture opening dimensions, although a clear trend with the internal overpressure at time of rupture can be discerned.

From the results presented in Table 4, we conclude that only small (< 1 mm) fuel fragments, created by rupture of grain boundary bubbles and HBS pores during the LOCA, are small enough to pass through the narrow breaches. The calculated pre-LOCA fuel fragment size is typically 1.8-1.9 mm in the axial segments where relocation occurs for the failed rods [25]. These fragments are clearly too large for passing through the cladding breach.

The dispersible fuel masses presented in Table 4 are upper bound estimates for the amount of fuel that could possibly be ejected into the coolant from the failed rods. As indicated in the table, these calculated masses correspond to 8.1-8.5 % of the total inventory of fuel in each rod. These calculated results for fuel dispersion may be compared with those of a simple empirical model, which is based on data for fuel fine fragmentation, relocation and dispersal observed in integral and semi-integral LOCA tests on high-burnup LWR fuel. The model is presented in different versions in appendix A of [13]. Here, we will make use of the version labelled 'model A'. It is based on the assumptions that all fuel fragments that are smaller than 1 mm and located in parts of the fuel rod where the cladding hoop strain exceeds 3 % are dispersed into the coolant. The fraction of fragments smaller than 1 mm is in the empirical model estimated through a simple correlation with pellet average burnup, which is applied to each axial segment that satisfies the aforementioned criterion on cladding hoop strain: this criterion defines where fuel axial relocation can take place. Results of the empirical 'model A' from [13] are included in Table 4 for comparison. On average for the four failed rods, the empirical 'model A' predicts that 7.8 % of the total fuel inventory is dispersed. This average fraction is very close to the results obtained from our model. However, the empirical 'model A' calculates large differences in fuel dispersal fractions among the four failed rods, primarily due to the differences in fuel burnup between them; see Table 3. The results calculated by our model are not that strongly dependent on fuel burnup. As will be shown in 3.3.2 below, the calculated extent of fuel fine fragmentation depends on fuel peak temperature in combination with burnup.

3.2.5. Axial gas flow and pressure gradients

Axial gas flow is known to be restricted in high-burnup LWR fuel rods [41-43]. This leads to axial pressure gradients as the fuel rod temperature distribution changes and/or the fuel and cladding deform [44]. These pressure gradients, which are neglected in most fuel performance analysis programs, are suspected to affect the fuel rod deformation and failure behaviour under LOCA [45].

In our analysis, axial gas flow and pressure gradients are considered by a computational model described in [28] and section B.1 of Appendix B. Here, we consider results calculated for the four rods that were predicted to fail; see Table 3. More precisely, the left panel of Fig. 17 shows the gas pressure difference between the top plenum and the axial position of cladding failure (z ~2.5 m), calculated versus time for the four failed rods. The rods show similar behaviour, in that significant axial pressure gradients are calculated to arise at three occasions during the LOCA: Firstly, during the blowdown phase (t < 10 s), when the gap gas pressure drops rapidly from fairly high pre-LOCA conditions as a combined result of decreasing fuel temperature and widening pellet-cladding gap. Secondly, during the ballooning phase (30 < t < 45 s), when the gap gas pressure in the balloon drops as a consequence of the increasing volume. Finally, just after cladding rupture (t > 298 s), when the cladding balloon is rapidly depressurized. For other parts of the failed rods, the final depressurization is fairly slow. For example, the calculated equilibration time for the plenum gas pressure is about 100 s, as evidenced by the left panel of Fig. 17.

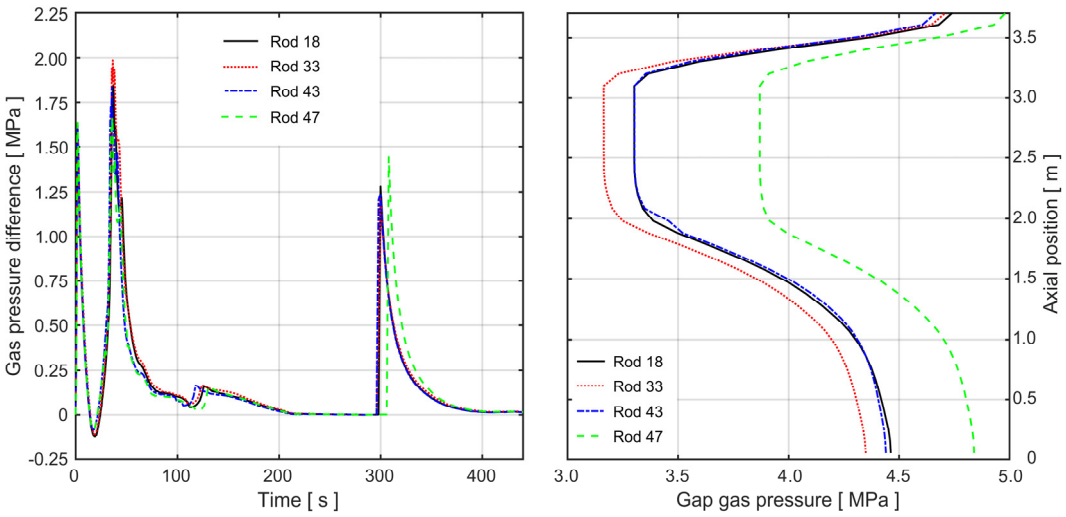

Fig. 17: Calculated gas pressure difference between top plenum and axial position of cladding failure (left), gap gas pressure versus axial position, calculated at t = 40 s (right).

It should be remarked that the cladding failures in the four rods occur at a time when the internal gas pressure is practically uniform. This is clear from the left panel of Fig. 17, which shows that no pressure differences exist between the plenum and the failure position from about t = 210 s to the time of cladding failure. This suggests that the failure process for the considered rods is not affected by restricted axial gas flow and pressure gradients. However, the situation would have been different, had the failures occurred during the ballooning phase, i.e. for 30 < t < 45 s. More precisely, the right panel of Fig. 17 shows the calculated variation in gap[1] gas pressure along the failed rods, calculated at t = 40 s. At this par-

[1] The figure also includes the plenum gas pressures, represented by the values shown for the top axial position (z = 3.7 m).

ticular time, the calculated cladding ballooning is at its final stage for the considered rods, and the local gas pressure in the ballooned part is low, due to the rapid volume increase. It is clear that the calculated gas pressure is uniform within the balloon ($2.1 < z < 3.1$ m), but that significant axial gradients exist towards the ends of the fuel rods. This indicates slow axial flow of gas from the large volume in the top plenum, corresponding to about 20 % of the total rod internal volume at $t = 40$ s, to the ballooning part. It is likely that both the rate and axial extent of ballooning are limited by the slow gas flow from the top plenum.

3.3. Post-LOCA fuel rod conditions

3.3.1. Fuel fragment axial relocation

The model for axial relocation of fuel fragments used in our analysis is fully described in [25], and its application to LOCA simulation tests is exemplified in [34, 46-48]. Since the model has proven successful for modelling tests with noticeable fuel relocation, it has been implemented in fuel performance codes used also by other organizations [49-51]. In short, the model assumes that local collapse of the cylindrical fuel pellet column into a disordered particle bed of fuel fragments takes place when the cladding local radial deformation (distension) is large enough that the ballooned volume is able to accommodate the crumbled and loosely packed fuel particles. The particle bed has a significantly lower fragment packing fraction (0.7-0.8) than the original cylindrical fuel pellet column (~1.0), and the effective thermal conductivity is also much lower [25]. In our model, the local packing fraction of fragments in each axial segment of the discretized fuel rod depends on the local fragment size distribution; see section B.3, Appendix B. This size distribution is calculated by our model for fuel fine fragmentation [21]; see section 3.3.2 below. Once the fuel pellet column is calculated to collapse into a crumbled state in an axial segment, downward axial relocation of fuel fragments from higher segments is calculated by the model, provided that the cladding distension in these higher segments is large enough to allow fragment detachment and axial movement [25]. The relocation is modelled as a dynamic process, where the axial re-distribution of fuel is calculated in each time step of the analysis, based on current cladding deformations and fuel fragment size distributions. However, in the following, we will consider only the calculated final post-LOCA conditions of the fuel pellet column.

The left panel of Fig. 18 shows that collapse of the fuel pellet column into a disordered bed of fuel fragments ("crumbling") is calculated to occur only for 22 fuel rods with pre-LOCA rod average LHGR higher than 15 kWm^{-1}. Due to the axial discretization of the fuel rod into 36 equal-length segments, the percentages in Fig. 18 correspond to fuel pellet crumbling in 1,2,6 or 7 of these axial segments. It is clear that the axial extent of fuel crumbling correlates with the pre-LOCA rod average LHGR.

The calculated post-LOCA distribution of fuel along each of the fuel rods is shown in the right panel of Fig. 18. Except for one rod that experiences limited ballooning and fuel relocation in only two axial segments ($2.9 < z < 3.0$ m), fuel fragments accumulate at the bottom ($2.4 < z < 2.8$ m) of the ballooned region. The relocated fragments originate from a section at the top ($2.9 < z < 3.1$ m) of the balloon, which is practically emptied of fuel at end of the postulated LOCA. The right panel of Fig. 18 shows only the final post-LOCA distribution of fuel, but our calculations show that the relocation starts close to the fuel peak power position (z ~3.0 m) and then progresses gradually downward in tandem with cladding ballooning.

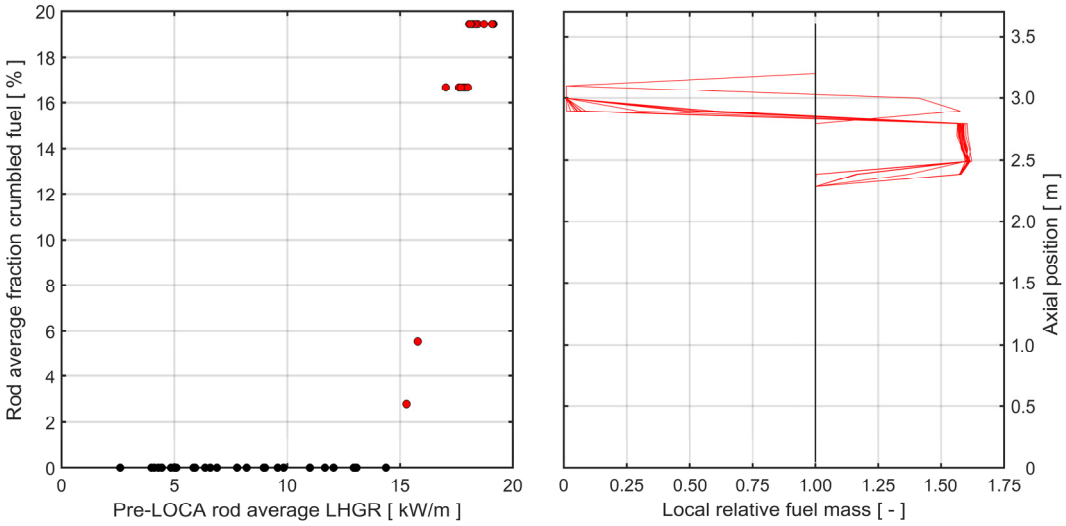

Fig. 18: Fraction of the fuel pellet column that experiences crumbling and fuel axial relocation (left), and post-LOCA distribution of fuel along the fuel rod (right).

Our analysis suggests that the fuel mass is locally increased by about 60 % in the lower part of the balloon, as a result of fuel fragment relocation. As shown in section 3.2.1, this has a significant effect on local heat load and cladding temperature. The local temperature escalation in turn increases fuel pellet fine fragmentation, transient fission gas release and cladding oxidation, as will be shown in sections 3.3.2-3.3.3 below. Yet, the local mass increase for the considered fuel rods is moderate in comparison with that for LOCA simulation tests [34], where the calculated and measured mass increase may reach 200 %. The reason is that the LOCA simulation tests are carried out in test rigs that allow the test rodlets to distend much more than what is possible in an LWR fuel assembly. In our analysis, the local mass increase is limited by rod-to-rod contact that constrains the cladding radial distension. Moreover, the calculated packing fraction of fuel fragments in the ballooned part of the rod is typically 0.77-0.78 in our analysis. This is a moderate packing fraction for the considered high-burnup fuel, which also limits the local mass increase in our analysis.

3.3.2. Fuel fine fragmentation and transient fission gas release

Fuel pellet fine fragmentation and transient fission gas release is in our analysis calculated by a model that attributes these phenomena to rupture of overpressurized grain boundary bubbles and/or HBS pores [21]. More precisely, the model combines analytical rupture criteria for these two types of gas cavities with submodels that are used for calculating the space-time evolution of average size, number density and gas content of the cavities. These submodels are implemented not only in FRAPTRAN-QT-1.5, but also in FRAPCON-QT-4.0P1, so that the long-term evolution of fuel microstructure can be modelled over the entire operating life of the fuel [21].

The left panel of Fig. 19 shows the calculated rod average fraction of finely fragmented fuel after the LOCA, plotted versus the rod average pre-LOCA LHGR. For rods with a pre-LOCA LHGR above 15 kWm^{-1}, there is a clear correlation between calculated rod average fine fragmentation and power, but for rods with a pre-LOCA LHGR less than 15 kWm^{-1}, there is no or negligible fragmentation. It is also evident from the figure that there is a significant spread in the calculated results for rods with pre-LOCA LHGR around 18 kWm^{-1}, which suggests that other parameters, such as fuel burnup, microstructure and pre-LOCA fission gas distribution, are important for the fine fragmentation.

From the right panel of Fig. 19, it is clear that the fine fragmentation occurs in the upper part of the fuel rod, where the highest temperatures are reached. The jagged appearance of the curves is caused by the fuel axial relocation and its effect on the fuel temperature evolution. The calculated peak radial average fraction of fine fuel fragments in any axial segment is 40-50 % for the fuel rods with highest rod average (~15 %) fine fragmentation.

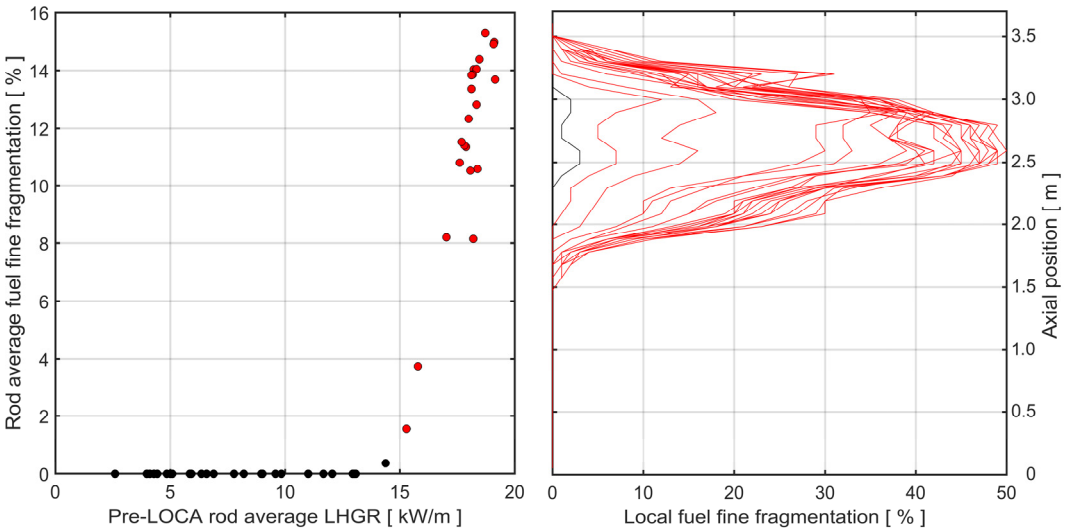

Fig. 19: Calculated post-LOCA rod average fraction of finely fragmented fuel versus pre-LOCA rod average LHGR (left). Local (radial average) post-LOCA rod average fraction of finely fragmented fuel versus axial position (right). Fuel rods that experience cladding ballooning and fuel axial relocation are marked in red.

The calculated relationship between fuel fine fragmentation and fuel peak temperature is shown in Fig. 20. More precisely, it show the calculated local (radial average) fraction of fine fuel fragments in each axial segment versus peak pellet surface temperature reached in the segment during the LOCA, plotted for all axial segments in all analysed rods. In axial segments with crumbled and relocated fuel, the surface temperature shown in the abscissa of Fig. 20 refers to the temperature at the periphery of the fuel particle bed, close to the cladding inner surface. The 36×50 data points are divided into three groups with respect to local (fuel pellet) burnup in the considered axial segment.

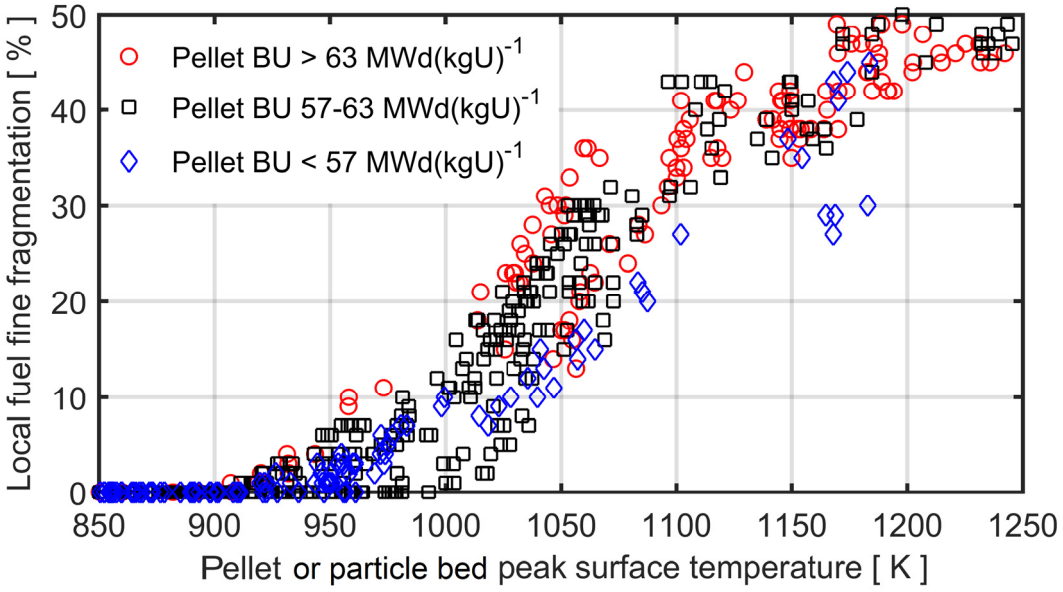

Fig. 20: Calculated relationship between local (pellet average) fuel fine fragmentation, pellet burnup and peak surface temperature reached during the LOCA.

From Fig. 20, it is clear that a peak surface temperature of 900-1000 K is needed for fuel fine fragmentation to occur in our calculations. This result is well in line with the empirical lower-bound temperature threshold for fuel fine fragmentation of 640 °C (913 K) that has been reported from annealing tests and laser heating tests on high-burnup fuel by Turnbull and co-workers [52]. The calculated extent of fuel fine fragmentation increases with increasing peak surface temperature, and the calculated results in Fig. 20 suggest a sigmoidal relationship.

The scatter in Fig. 20 indicates that there are other parameters than peak temperature that affect the extent of fine fragmentation. One likely parameter is fuel burnup, and an attempt to graphically identify trends with regard to fuel burnup has been made by dividing the data in Fig. 20 into three categories. However, no clear trends with regard to burnup can be discerned in Fig. 20. This has been veri-

fied quantitatively by calculating partial rank correlation coefficients[2] between the calculated extent of local fuel fine fragmentation in Fig. 20 and the peak pellet surface temperature and pellet burnup, respectively. The correlation coefficient between fuel fine fragmentation and peak pellet surface temperature is 0.611, whereas the correlation coefficient between fine fragmentation and burnup is only 0.013. The corresponding p-values are 0 and 0.589, respectively. These numbers reveal that the calculated fuel fine fragmentation has a statistically significant relationship with the peak pellet surface temperature, but not with pellet burnup.

To elucidate this surprising result, the same data as in Fig. 20 are plotted versus pellet burnup in Fig. 21. From the latter figure, it is clear that there is a threshold burnup for the calculated fuel fine fragmentation, but this threshold is only seen in axial segments with a peak fuel surface temperature, T_s, lower than 1050 K. There are simply no data points for peak fuel surface temperatures above 1050 K and pellet burnups less than 53 MWd(kgU)$^{-1}$, so the expected burnup threshold is unobservable in these high-temperature data.

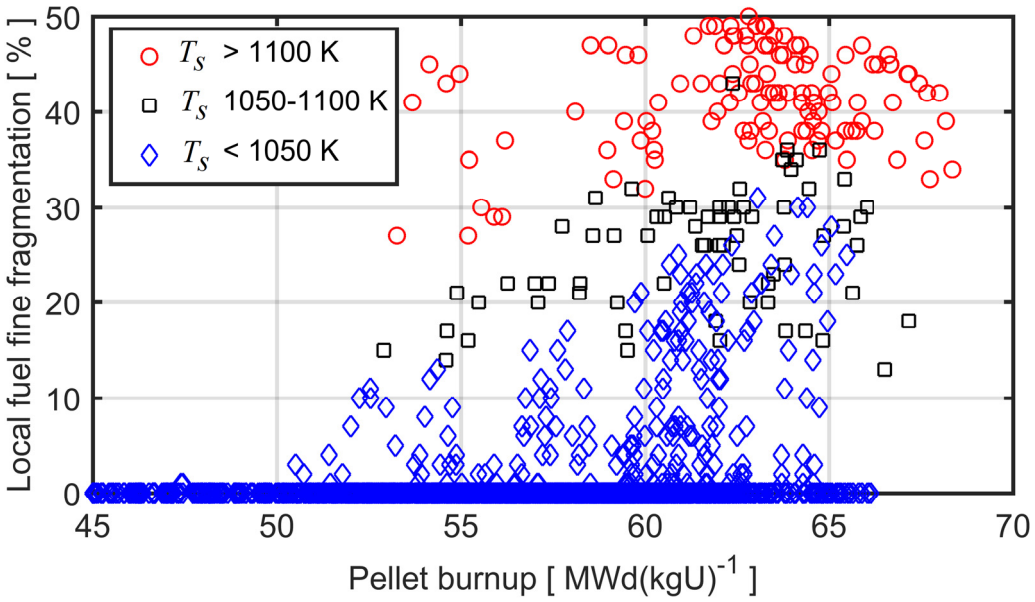

Fig. 21: Calculated relationship between local (pellet average) fuel fine fragmentation, pellet burnup and peak surface temperature (T_s) reached during the LOCA.

Finally, it must be recognized that the peak surface temperature used as abscissa in Fig. 20 is a rather crude measure of the thermal load experienced by the fuel during LOCA, since it does not account for the differences in radial temperature

[2] A partial rank correlation coefficient, also known as Spearman's partial correlation coefficient, indicates the degree of monotonicity between a specific input variable and an outcome (here the extent of fuel fine fragmentation), with the effects of other input variables removed [53]. The corresponding p-value indicates the probability that the calculated correlation coefficient ocurred by chance.

distribution between axial segments with crumbled and relocated fuel in a particle bed versus axial segments where the cylindrical fuel pellet column is intact.

Since the applied model assumes that fine fragmentation of the fuel material leads to transient fission gas release, the calculated gas release follows the same trend as the fine fragmentation; compare Fig. 19 with Fig. 22.

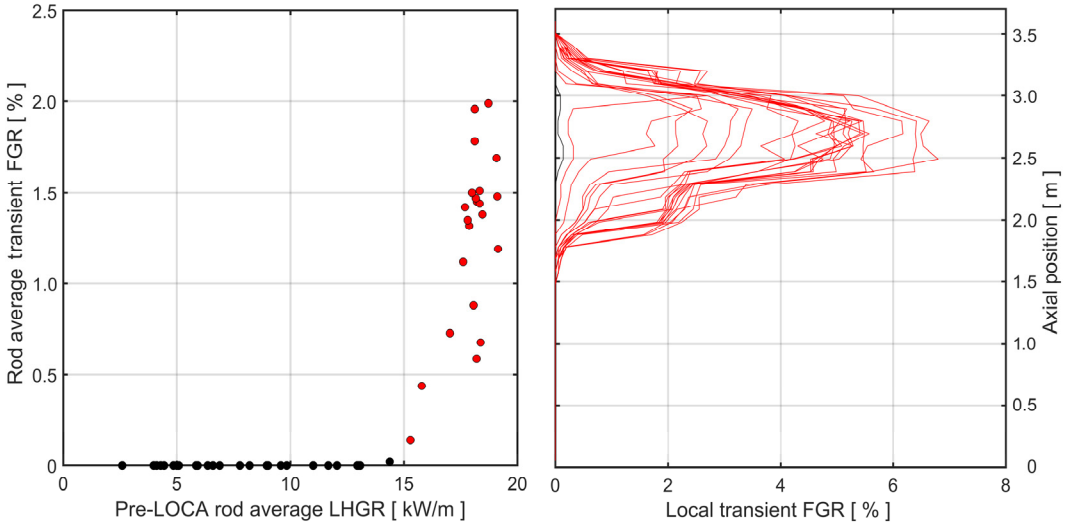

Fig. 22: Calculated rod average transient fission gas release versus pre-LOCA rod average LHGR (left). Local (pellet average) transient fission gas release versus axial position (right).

From Fig. 22, it is clear that the calculated rod average gas release under the postulated LOCA is less than 2 % for all rods, and that the local (pellet average) transient gas release does not exceed 7 % in any of the analysed fuel rods. These values, which are in line with experimental data [54] and calculated results [55] for high-burnup fuel under LOCA, are fairly moderate, and the increase in post-LOCA internal gas pressure caused by transient gas release is less than 15 %. However, the local relative increase in gas pressure in the hot, ballooning, part of the rod is momentarily higher just when the gas is released, since pressure equilibration by axial gas communication with the top plenum is slow. This can be seen by "bumps" in the calculated time histories for the overpressure in the ballooning part of the rods; see the right panel of Fig. 14. The calculated gas release contributes to the cladding ballooning by increasing the rod internal pressure locally.

We recall from section 3.1.3 that some fission gas was released by thermal processes already before the LOCA, according to our calculations. This is illustrated for the four failed rods in the left panel of Fig. 23, which shows the pre-LOCA fission gas release across the fuel pellet, calculated at the axial position of cladding failure (z ~2.5 m). It is clear that significant thermal gas release has occurred from the central part of the pellets at this axial position, and that some gas has also been released by athermal mechanisms from the restructured material at the pellet surface: the calculated extent of high-burnup UO_2 restructuring is shown in the right panel of Fig. 23. The calculated extent of restructuring, including the width

of the so-called rim zone, correlates with fuel burnup. The model used for calculating UO_2 restructuring and the athermal fission gas release associated with the process is described in [21].

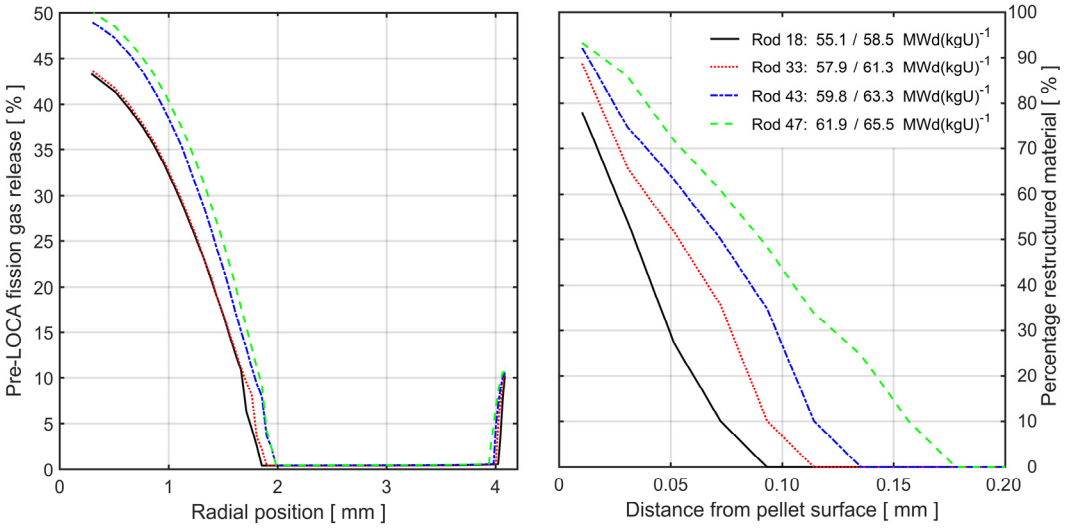

Fig. 23: Calculated pre-LOCA fission gas release versus radial position for the failed rods (left) and calculated extent of high-burnup UO_2 restructuring at the pellet surface (right). The results pertain to the axial position of cladding failure. The legend indicates the rod average and local (pellet average) burnup.

Our calculations suggest that the fission gas released during the postulated LOCA originates from three different annular regions, as shown in the left panel of Fig. 24. From the innermost region ($0.8 < r < 1.9$ mm), gas is transiently released through a network of interconnected grain boundary bubbles. This network has formed long before the LOCA, and it is responsible for the pre-LOCA fission gas release shown in the left panel of Fig. 23. During the postulated LOCA, the network once again serves as a release path for fission gas. However, no transient fission gas release occurs trough the network from the central part of the fuel pellets ($r < 0.8$ mm), since the fuel temperature in this part is significantly lower during the LOCA than under the pre-LOCA operating conditions.

From the intermediate region ($2.8 < r < 4.0$ mm), the transient fission gas release is calculated to occur by grain boundary fracture and pulverization of the material. Both the aforementioned processes result in about 4 % local transient gas release, originating from grain boundary bubbles. Higher release fractions are calculated from the outermost region, which consists of the outer half of the restructured rim zone: compare the right panels of Fig. 23 and Fig. 24. The gas release is calculated to occur by rupture of overpressurized pores in the restructured material. This rupture takes place only in the outer half of the rim zone, where the size, number density and gas content of the pores are sufficient for breaking the material by the pore overpressure reached during the temperature excursion.

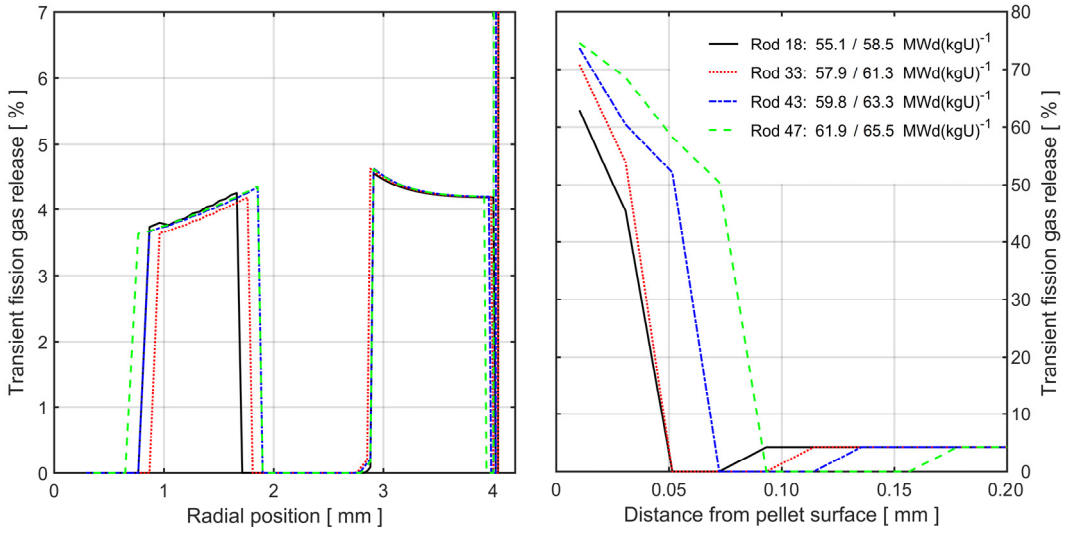

Fig. 24: Calculated transient fission gas release versus radial position for the failed rods. The results pertain to the axial position of cladding failure. The legend indicates the rod average and local (pellet average) burnup.

3.3.3. Cladding high-temperature oxidation

The state of cladding corrosion before the LOCA, calculated by use of existing models for Optimized ZIRLO in FRAPCON-4.0P1 [22], was presented in section 3.1.2. During the postulated LOCA, some of the considered fuel rods reach sufficiently high temperature (> 1100 K) that the cladding is further oxidized in the upper part of the core. This is illustrated by Fig. 25 and Fig. 26, which show the equivalent cladding reacted (ECR). The ECR is a cladding degradation parameter that is widely used in acceptance criteria for emergency core cooling systems. It is defined as the percentage of the cladding thickness that would be oxidized, if all the oxygen from the cladding-water reactions stayed in the oxide layer as ZrO_2.

The ECR shown in Fig. 25 is the *total* oxidation of the cladding, caused by both long-term cladding corrosion during normal operation before the LOCA and high-temperature oxidation during the accident. The left panel of Fig. 25 shows the maximum post-LOCA ECR with regard to axial position for each fuel rod, whereas the right panel shows the axial variation along each rod. Obviously, the peak total ECR among the rods is about 8.5 % and the peak is reached in the upper and/or lower part of the balloon. The peaks are caused not only by high local temperature, but also by local wall-thinning of the ballooning cladding: the ECR (cladding wall thickness fraction) is calculated with respect to the deformed cladding thickness.

The peak ECR reached during pre-LOCA normal operation is calculated to about 4 %, and the peak is in the region $3.1 < z < 3.3$ m; see the left panel of Fig. 6. High-temperature oxidation during LOCA is calculated to add at most 4.5 % to the total ECR at the axial peak position: this is clear from the left panel of Fig. 26, which shows the calculated LOCA-induced ECR along each fuel rod.

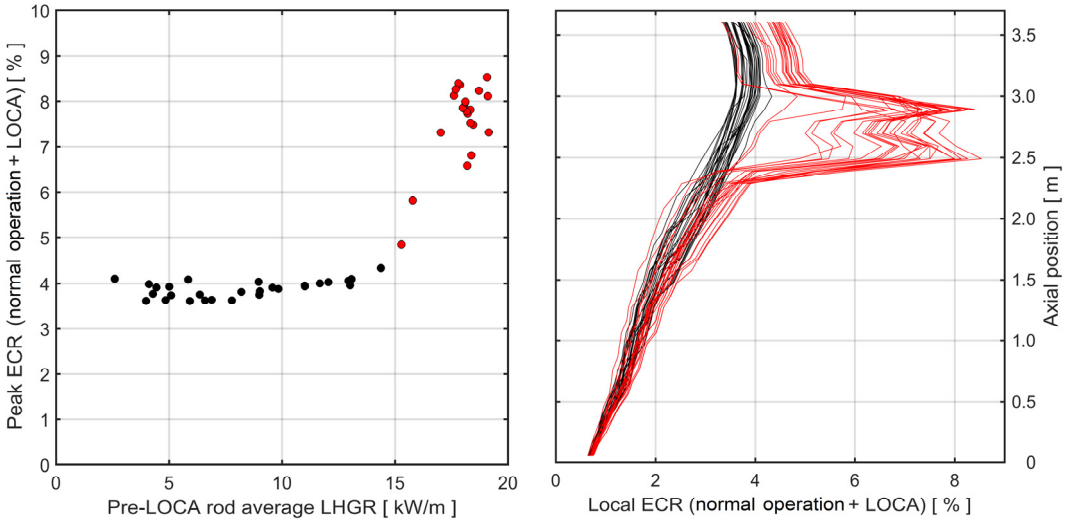

Fig. 25: Calculated post-LOCA equivalent cladding reacted (ECR), including both cladding corrosion during pre-LOCA normal operation and high-temperature oxidation during the postulated accident. Fuel rods that experience cladding ballooning and fuel axial relocation are marked in red.

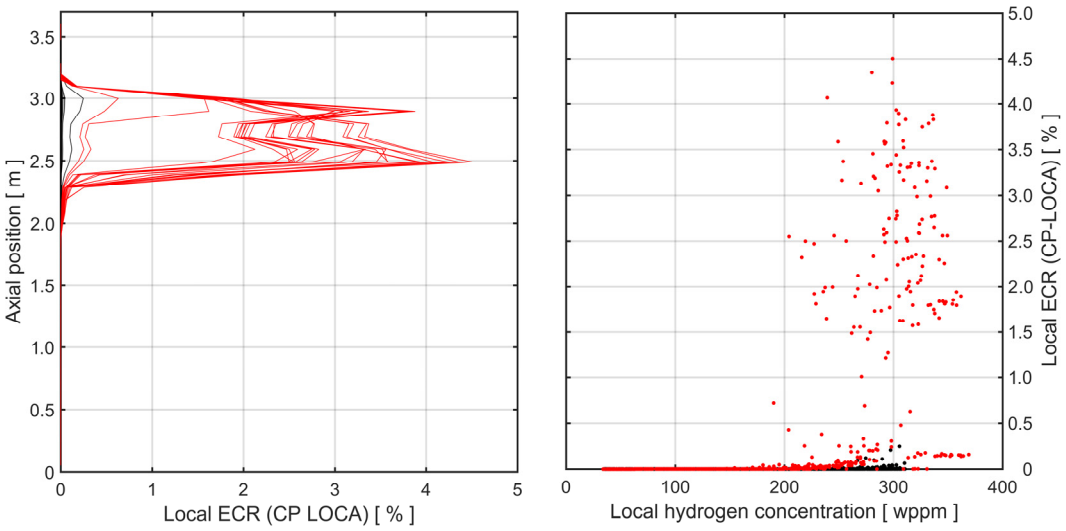

Fig. 26: Local LOCA-induced ECR, calculated with the Cathcart-Pawel high-temperature oxidation model [33], versus axial position (left) and local pre-LOCA hydrogen concentration in the cladding (right).

Acceptance criteria for LOCA generally include limits for the maximum allowable ECR reached during the accident as a result of high-temperature oxidation. Detrimental effects of pre-LOCA long-term cladding corrosion are considered by defining the limits for the LOCA-induced ECR as decreasing functions of cladding hydrogen concentration; see e.g. [56, 57] and references therein. In the right panel of Fig. 26, the calculated LOCA-induced ECR in each axial segment of the fifty analysed fuel rods is plotted versus the calculated pre-LOCA cladding hy-

drogen concentration for the segment. Two comments should be made on this figure: Firstly, the calculated LOCA-induced ECR is well below the acceptance criteria defined in [56, 57]. Secondly, the highest calculated ECR is not obtained in axial segments with the highest calculated hydrogen concentration. This can be understood by comparing the right panel of Fig. 6 with the left panel of Fig. 26: the peak LOCA-induced ECR is in the considered fuel rods reached at a somewhat lower position (~2.5 m) than the peak hydrogen concentration (~3.2 m). The fact that the two peaks do not coincide is deemed beneficial for cladding ductility, and hence, for the cladding tube survivability during quench.

Finally, it should be remarked that double-sided oxidation of the cladding, close to the cladding breach, has a negligible effect on the calculated results for the four failed fuel rods. The reason is that the failures occur late in the accident, when the temperature has decreased to about 1070 K; see Table 4.

4. Conclusions and outlook

In section 4.1 below, we briefly summarize the most important results from the best-estimate analyses in section 3. Emphasis is placed on the results related to FFRD – fuel fragmentation, relocation and dispersal. For the analysed accident scenario, these high-burnup phenomena are calculated to occur in some of the considered fuel rods. Section 4.2 contains the results of parametric studies and sensitivity analyses, intended to supplement the best-estimate analyses by quantifying the impact of model parameters and modelling assumptions, including the accident scenario. Finally, in section 4.3, we identify and discuss shortcomings of the presented analyses and make suggestions for further work.

4.1. Summary and interpretation of calculated results

4.1.1. Pre-LOCA fuel rod conditions

The fuel rods analysed in this work are fifty selected real-world fuel rods that were discharged in 2022 after completing cycle 39 in the Ringhals 4 PWR, Sweden. The calculated average burnup of the selected rods ranges from 49 to 63 $MWd(kgU)^{-1}$, while the peak pellet burnup is 53-69 $MWd(kgU)^{-1}$.

The calculated cladding corrosion is deemed typical for discharged PWR fuel rods of this generation: the calculated end-of-life peak oxide layer thickness is 27-38 μm and the peak hydrogen concentration ranges from 270 to 375 wppm for the rods under study. The most corroded part of the cladding is found about 0.4 m below the upper end of the fuel pellet column.

The large-break LOCA is postulated to occur at end of cycle 39 in Ringhals 4, i.e. at end-of-life conditions for the analysed fuel rods. When the LOCA initiates, the rods have average linear heat generation rates between 2.6 and 19.2 kWm^{-1} and the calculated pre-LOCA internal gas pressure ranges from 7.2 to 11.6 MPa. The calculated pre-LOCA rod average fission gas release is between 1 and 5 % for the analysed rods, and the gas release correlates with the rod lifetime average linear heat generation rate, which is in the range from 17 to 25 kWm^{-1}.

Even though the calculated pre-LOCA fission gas release is moderate for the considered rods, it increases the rod internal gas pressure at onset of the postulated LOCA by up to 30 %. This pressure increase is detrimental to the survivability of the fuel rods during the accident, and the calculated risk for cladding failure is correlated to the pre-LOCA fission gas release and hence, to the rod lifetime average linear heat generation rate; see section 4.2.1 below.

4.1.2. LOCA fuel rod conditions

In line with other studies of this kind, our calculations show that the pre-LOCA rod average LHGR has a very strong effect on virtually all aspects of the fuel rod behaviour under the postulated LOCA: temperatures, deformations, cladding oxidation and damage, as well as fuel pellet fine fragmentation, axial relocation and transient fission gas release. This is further discussed in section 4.2.1 below.

The calculations suggest that fuel rods operating with an average LHGR below 15 kWm^{-1} when the LOCA occurs experience negligible deformation, oxidation and damage during the postulated accident. For fuel rods with higher pre-LOCA power, the calculated cladding deformations are sufficient to cause local collapse of the fuel pellet column and axial relocation of the crumbled fuel. According to our calculations, the relocation has a strong detrimental effect on the fuel rod behaviour, primarily through the local increase in fuel and cladding temperature that the relocation brings about; see section 3.2.1. This temperature increase, in turn, increases fuel pellet fine fragmentation and transient fission gas release, as well as cladding oxidation and damage; see section 4.2.2 below. In fact, the fuel fragment axial relocation induces a clear threshold effect for these phenomena, since the calculations show large differences between rods that experience relocation and those that do not. This is clear from the left panels of Fig. 15, Fig. 19 and Fig. 22.

Considering the strong detrimental effects of fuel fragment relocation calculated in this work, it should be pointed out that cautious assumptions were made for the relocation modelling. Firstly, the cladding tube distension is assumed to be restricted by contact with neighbouring fuel rods, which limits the cladding hoop strain to about 32 %. Secondly, the packing fraction of crumbled fuel that accumulates in the ballooned part of the fuel rod is typically 0.77-0.78 in our analyses, which is in line with existing data for crumbled fuel with a pellet average burnup around 65 $MWd(kgU)^{-1}$ [13]. These two assumptions combined result in a local fuel mass increase of no more than about 60 % in the ballooned part of the fuel rod, which is moderate in comparison with results from a recent computational study on PWR LB LOCA by the Korean Institute of Nuclear Safety [49].

Four of the fifty analysed fuel rods are calculated to fail during the postulated LOCA. These are the four rods with the highest pre-LOCA rod average LHGR in the population, more precisely 18.7-19.2 kWm^{-1}. The average burnup of the failed rods ranges from 55 to 62 $MWd(kgU)^{-1}$ and the calculations show no obvious effect of burnup on the failure behaviour among these rods. The failure is calculated to occur in the lower part of the ballooned region for all four rods, and somewhat surprisingly, all of them are calculated to fail late in the postulated accident. The late failures are caused by localized embrittlement of the cladding, resulting from prolonged high-temperature oxidation in the lower part of the balloon, combined with increasing hoop stress in the cladding as temperature decreases and thermal contraction leads to relaxation of rod-to-rod contact forces; see section 3.2.3. To the author's best knowledge, late cladding failures of this kind have not

been observed in LOCA simulation tests: reported failure modes are either ductile failure (burst) by rod internal overpressure at high temperature, or brittle failure of severely oxidized cladding by thermal stresses induced upon quenching [1]. Hence, there is reason to question whether the failure mode in our calculations is realistic.

Since the calculated failures are of brittle nature, the calculated rupture openings are small and crack-like: best-estimates for the tangential width and the axial length of the cladding breaches range from 1.0 to 1.3 mm and 7.3 to 8.3 mm, respectively. Only small fuel fragments, formed mainly by gas-induced pulverization of the fuel pellets during the LOCA, are likely to pass through these narrow breaches. As described in section 3.2.4, upper bound estimates for the amount of fuel fragments that can possibly be dispersed into the coolant are made by comparing the best-estimate cladding breach dimensions with calculated results from our models for fuel fine fragmentation and axial relocation. The estimated amount ranges from 165 to 172 g UO_2 for the failed rods, which corresponds to 8.1-8.5 % of the total rod inventory. These values are in line with results from empirical models proposed for fuel dispersal estimates [13].

Our analyses suggest that significant axial gradients in rod internal gas pressure arise when the fuel rod temperature distribution is rapidly changed and/or the cladding tube distends locally; see section 3.2.5. In particular, the flow of gas from the rod upper plenum to the hot ballooning part of the rod is slow, which limits both the rate and axial extent of ballooning. Hence, the prevalent assumptions of unrestricted axial gas flow and instantaneous gas pressure equilibration in LOCA fuel rod analyses are probably conservative with regard to cladding deformation.

During the postulated accident, transient fission gas release is calculated to occur in fuel rods with a pre-LOCA rod average LHGR above 13 kWm^{-1}. The calculated gas release is axially concentrated to the hot, ballooning, part of the fuel rods, and our calculations show that a pellet surface temperature of at least 900-1000 K is required to trigger the release. With regard to radial position in the fuel pellet, the transient gas release is calculated to occur by rupture of overpressurized HBS pores and grain boundary bubbles in the peripheral part of the pellet, but in some cases also by venting of grain boundary bubbles through existing (pre-LOCA) release paths in more central parts of the pellet; see section 3.3.2. The former gas release mechanism is in our model closely related to fine fragmentation of the fuel material. This fragmentation is calculated to occur only in the hot, ballooning, part of the fuel rods, and there is a clear correlation between the calculated degree of fine fragmentation and the peak pellet surface temperature. The calculated fraction of finely fragmented fuel reaches at most about 50 % in the hottest axial segments, while the highest rod average fraction of fine fragments is about 15 %. The calculated influence of pellet burnup on fuel fragmentation is weak, but as explained in section 3.3.2, this is mainly due to the fact that most of the calculated fragmentation occurs in severely overheated pellets with burnups from 55 to 65 $MWd(kgU)^{-1}$. Calculated effects of fuel burnup, as such, are not evident at high temperature within this fairly narrow burnup span.

The waterside cladding corrosion reached in normal service before the LOCA corresponds to at most 4 % equivalent cladding reacted (ECR) locally in the most corroded fuel rod. High-temperature cladding oxidation during the postulated LOCA is calculated to add at most 4.5 % to the total ECR. As a result of fuel axial relocation and the downward shift of peak temperature that the relocation brings about, the LOCA-induced oxidation is peaked to a lower part of the fuel rod than the pre-LOCA corrosion. The fact that the two peaks do not coincide is deemed beneficial for the cladding survivability during quench; see section 3.3.3.

4.2. Parametric studies and sensitivity analyses

4.2.1. Impact of pre-LOCA fuel rod conditions

As already mentioned, it is clear from the calculated results in sections 3.2 and 3.3 that the pre-LOCA rod average LHGR has a very strong effect on the calculated fuel rod behaviour under the postulated LOCA: peak temperatures, cladding deformation, oxidation and damage, as well as fuel pellet fine fragmentation, axial relocation and transient fission gas release are all strongly correlated to the pre-LOCA LHGR. On the other hand, possible effects of fuel burnup or other pre-LOCA fuel rod conditions on these performance parameters are not obvious from the calculated results and should therefore be further investigated.

To this end, we have calculated partial rank correlation coefficients between three parameters that are deemed to characterize the pre-LOCA state of the fuel rod and five selected parameters that characterize the fuel performance under the LOCA. A partial rank correlation coefficient, also known as Spearman's partial correlation coefficient, exists in the interval from -1 to +1. The value indicates the degree of monotonicity between a specific input variable and an output variable, with the effects of other input variables removed [53]. The higher the value, the stronger is the correlation between the two variables: positive values indicate an increasing monotonic trend, while negative values correspond to a decreasing trend between input and output. Low ($< |0.25|$) values are not statistically significant. The significance can be quantified with Student's t-test, which gives the probability (p-value) that the calculated correlation coefficient ocurred by chance [53].

Here, the pre-LOCA (input) parameters deemed important for the fuel rod behaviour under the accident are the rod average burnup, the rod average LHGR at onset of LOCA, and the rod lifetime average LHGR. The five selected performance (output) parameters are the space-time maxima for cladding temperature, damage index and LOCA-induced ECR, and the rod average post-LOCA fractions of fine fuel fragments and transient fission gas release. The partial rank correlation coefficients between these input and output parameters, calculated for a population consisting of the fifty analysed fuel rods, are presented in Table 5. The p-value for each correlation coefficient is given in brackets. Moreover, correlation coefficients with a p-value less than 0.10 are marked with green colour in Table 5. These correlation coefficients are deemed statistically significant.

Table 5: Calculated partial rank correlation coefficients between three pre-LOCA fuel rod state parameters (top) and five output parameters (left). The corresponding p-value for each coefficient is given in brackets. Correlation coefficients with $p < 0.1$ are considered statistically significant and marked in green colour.

	Fuel rod pre-LOCA state parameter		
Performance parameter	**Rod average burnup**	**ALHGR at onset of LOCA**	**Lifetime average ALHGR**
Peak cladding temperature	**0.185** (0.208)	**0.989** (0)	**0.415** (0.003)
Peak cladding damage index	**0.388** (0.006)	**0.980** (0)	**0.388** (0.007)
Peak LOCA-induced ECR	**0.107** (0.471)	**0.689** (0)	**0.154** (0.296)
Rod average fuel fragmentation	**0.233** (0.112)	**0.757** (0)	**0.031** (0.834)
Rod average transient FGR	**0.255** (0.081)	**0.677** (0)	**0.144** (0.329)

The partial rank correlation coefficients in Table 5 confirm our previous conclusions: the rod average LHGR at onset of LOCA has a clear effect on all aspects of the calculated fuel rod behaviour under the postulated LOCA, while rod average burnup and rod lifetime average LHGR have only modest impact. We recall from section 3.1.3 that the latter parameter has a notable effect on the fuel rod pre-LOCA fission gas release and rod internal gas pressure, which in turn affect the peak cladding temperature and damage index reached during the accident.

4.2.2. Impact of fuel axial relocation

In section 3.2.1, we presented results from a parametric study, in which our model for fuel axial relocation was deactivated. From this study, we concluded that axial relocation of fuel fragments, if it occurs, has a significant amplifying effect on local fuel and cladding temperatures in the lower part of the balloon, where the relocated fragments accumulate. The relocation also shifts the axial position of peak temperature downward, which in the analysed accident scenario is beneficial with regard to the pre-LOCA state of cladding corrosion. Here, we will extend the discussion to other parameters than fuel and cladding temperatures.

As shown in Fig. 12, the calculated increase in cladding temperature caused by fuel axial relocation is significant for several minutes under the postulated accident. During this period, the cladding oxidation is accelerated by the elevated temperature. The left panel of Fig. 27 shows the calculated relative change in peak cladding temperature and peak LOCA-induced ECR that the fuel relocation brings about for the 22 fuel rods that are calculated to experience relocation during the

postulated accident. The relative increase in PCT is below 15 % (compare with Fig. 11), while the LOCA-induced ECR increases as much as 130 %.

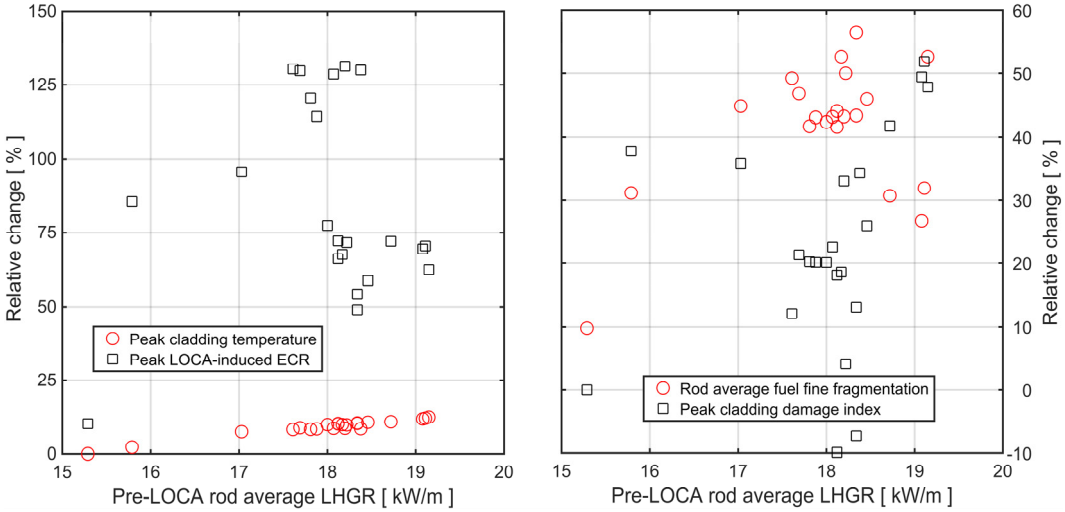

Fig. 27: Calculated effects of fuel fragment axial relocation in 22 of the analysed fuel rods. Left panel: Relative change in peak cladding temperature and LOCA-induced ECR. Right panel: Relative change in peak cladding damage index and post-LOCA rod average fraction of fine fuel fragments.

The combined effects of increased cladding temperature and oxidation that result from fuel axial relocation deteriorate the cladding high-temperature strength. More precisely, the predicted cladding burst stress decreases with both temperature and oxygen concentration in the cladding metal layer; see section B.2 in Appendix B. The calculated effect of fuel axial relocation on the peak cladding damage index is shown in the right panel of Fig. 27. The calculated relative increase is up to 52 %, but there are also two rods, for which the damage index is calculated to decrease by 8-10 % as a result of the relocation. This rather unexpected result is due to a reduction in rod internal gas pressure, caused by relocation-enhanced ballooning, during the early phase of the LOCA.

The fuel axial relocation has a significant amplifying effect also on calculated fuel pellet temperatures, which in our analyses enhances fuel fine fragmentation by rupture of overpressurized grain boundary bubbles and HBS pores. As shown in the right panel of Fig. 27, the post-LOCA rod average fraction of fine fuel fragments is calculated to increase by up to 58 %, as a result of fuel axial relocation.

4.2.3. Impact of postulated accident scenario

The fuel rod analyses presented in this report are done with thermal-mechanical boundary conditions, calculated for a specific LB LOCA scenario [18]. The scenario, which results in a prolonged period with high temperatures, is considered challenging (conservative) with regard to fuel rod damage; see section 2.1.

The scenario is adequate for our study, since many of the high-burnup phenomena that we set out to investigate are triggered by the high temperatures reached in fuel rods with pre-LOCA rod average LHGR above 15 kWm^{-1}. However, the question is to what extent these phenomena manifest themselves also in less challenging accident scenarios?

In an attempt to answer this question, supplementary fuel rod analyses were carried out with thermal-mechanical boundary conditions pertaining to an accident scenario more representative for what is used in the Ringhals 4 Final Safety Analysis Report (FSAR). These boundary conditions were provided as confidential information by Ringhals AB and Vattenfall Nuclear Fuel AB. They are similar to boundary conditions in best-estimate plus uncertainty (BEPU) methodologies that are typically used in plant safety analysis report for representative fuel rods with near end-of-life burnups. The boundary conditions, as well as results from our supplementary fuel rod analyses with these boundary conditions, are presented in Appendix D (confidential). Here, we will merely summarize key results and compare them with results for the base case hitherto analysed in this report. It should be remarked that only the fuel rod thermal-mechanical boundary conditions for the postulated LOCA, i.e. the space-time dependent coolant pressure, coolant temperature and cladding-to-coolant heat transfer coefficient, differ between the two analysed cases: the analysed fuel rods are exactly the same, and so are the applied computational models.

Fig. 28 shows calculated time histories of cladding peak temperature for the fifty analysed fuel rods. Results from the supplementary analyses are compared with those from the base case; compare with Fig. 10. As expected, the calculated temperatures from the supplementary analyses are significantly lower than those from the more challenging base case, and the temperature excursion ends about 100 s earlier. Although the supplementary analyses show a significant heat-up during the blowdown phase ($t < 10$ s), which is not seen in the base case scenario, the calculated cladding temperatures during this phase are not high enough to cause cladding plastic deformation. Hence, the early temperature peak has no lasting effect on the fuel rod behaviour.

In the supplementary analyses, fuel axial relocation is not calculated for any of the fuel rods. The reason is that the calculated cladding deformation is insufficient to cause collapse of the fuel pellet column at any stage of the postulated accident.

Peak values of selected fuel performance parameters, calculated with the two sets of thermal-mechanical boundary conditions, are compared in Table 6. The peak values are evaluated over the entire population of (50) fuel rods. The large differences in calculated peak values between the two cases in Table 6 give evidence that the thermal-mechanical boundary conditions are decisive for the fuel rod performance. As already mentioned in section 4.1.2, our calculations show a clear breakpoint in the fuel rod behaviour for cases where the temperature gets high enough to induce cladding ballooning and subsequent fuel axial relocation. This breakpoint is not reached for the temperatures calculated with the boundary conditions in the supplementary case.

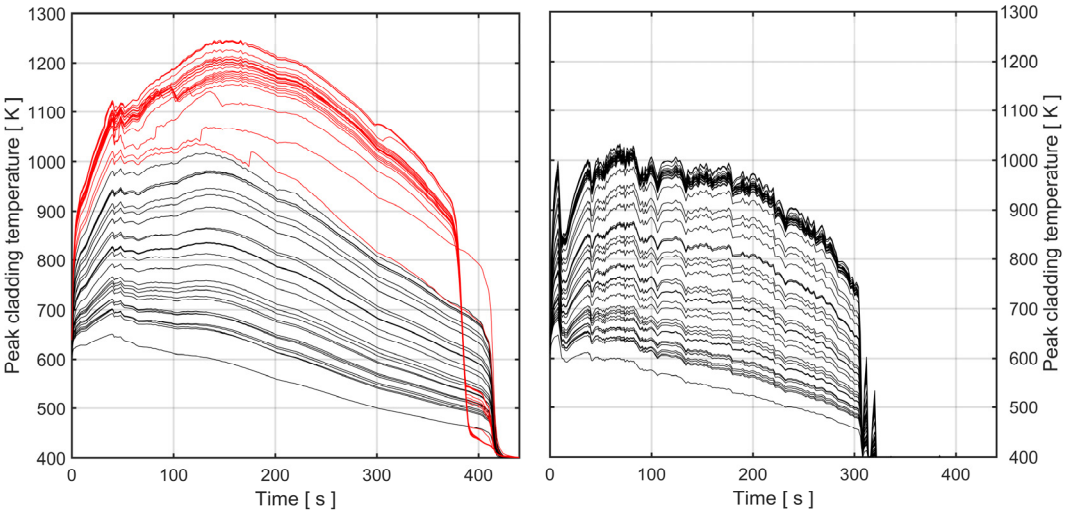

Fig. 28: Peak cladding temperature, calculated versus time for each of the fifty fuel rods, using thermal-mechanical boundary conditions from base case (left) and supplementary case (right). Red curves indicate fuel rods, for which cladding ballooning, fuel pellet column collapse and axial relocation of fuel fragments are calculated.

Table 6: Peak values of selected fuel performance parameters, calculated with the two sets of thermal-mechanical boundary conditions.

Peak value of fuel rod LOCA performance parameter		**Base case**	**Supplementary case**
Cladding temperature	[K]	1245.5	1033.5
Cladding damage index	[%]	100.0	32.6
Cladding hoop strain	[%]	31.8	6.6
Cladding LOCA-induced ECR	[%]	4.5	0.0
Rod average fuel fine fragmentation	[%]	15.3	2.1
Rod average transient FGR	[%]	2.0	0.2

4.3. Suggestions for further work

Throughout this report, the fuel rod LOCA analyses are carried out with fixed thermal-mechanical boundary conditions in the form of pre-calculated space-time dependent data for coolant pressure, coolant temperature and cladding-to-coolant heat transfer coefficient. The same boundary condition data are applied to all fuel rods, irrespective of their burnup and power, and possible feedback effects from the calculated fuel rod behaviour to the space-time variation of the aforementioned coolant properties are neglected. In particular, the applied methodology does not account for possible feedback effects from cladding ballooning and fuel axial relocation on coolant local temperature and cladding-to-coolant heat trans-

fer. To properly account for these feedback effects, the fuel rod analysis program should be integrated with the core and coolant system analysis software.

Most of the transient fuel rod analyses presented in this work are done with thermal-mechanical boundary conditions pertaining to a postulated LOCA scenario that results in challenging conditions with regard to fuel rod damage. Results from supplementary analyses, carried out with boundary conditions for a milder accident scenario, are presented in Appendix D and summarized in section 4.2.3. Considering the large differences in calculated fuel rod behaviour between these scenarios, it would be valuable to study the impact of fuel rod thermal-mechanical boundary conditions further. This could be done either by adding postulated accident scenarios to the analyses, or by performing parametric studies for a given scenario.

Our modelling with FRAPTRAN-QT-1.5 is geometrically restricted to single fuel rods with axisymmetric design and initial conditions, subjected to axially symmetric boundary conditions for the postulated accident. Moreover, the axial symmetry is assumed to be maintained throughout the accident. This assumption is simplistic, in particular for fuel rods that undergo ballooning [1], and it is therefore likely that the internal volume of the balloon is underestimated in our analyses. If so, the fuel axial relocation would be underestimated and the rod internal gas pressure in the ballooning region overestimated.

Although FRAPTRAN-QT-1.5 is restricted to single fuel rods, mechanical constraint from rod-to-rod contact is modelled. However, due to the assumption of axial symmetry, this modelling is inevitably simplistic. For example, mechanical constraint from rod-to-rod contact is in the radial direction modelled by limiting the diameter of the distended fuel rod to the rod-to-rod pitch of the fuel assembly. In order to model rod deformations and rod-to-rod thermal-mechanical interaction with higher fidelity, multi-rod modelling in three dimensions (3D) is needed. To the author's best knowledge, computational tools with this capacity are rare: examples include the outdated multi-rod code FRETA-B from the 1980s [58, 59], and the up-to-date DRACCAR computational platform [60, 61]. The latter couples a general-purpose program for thermo-hydraulic analysis of a fuel assembly (or part thereof) with a designated program for thermal-mechanical analysis of several thermally and mechanically interacting fuel rods, guide tubes and control rods in the considered geometry. The program for thermal-mechanical analysis uses a quasi-3D model, in which the lateral (2D) deformations of all rods included in the model are calculated in a stack of axial segments [60, 61].

Finally, it should be remarked that all fuel rod analyses presented in this report are done without considering the effects of spacer grids on cladding deformation. Results from a LOCA simulation program in the early 1980s, where assemblies of full-length PWR fuel rods were tested in the Canadian NRU reactor [62], show that cladding ballooning is significantly restrained at spacer grid positions. More recent single-rod LOCA simulation tests in the MIR [10] and Halden [63, 64] research reactors show similar results. It is therefore reasonable to believe that spacer grids will act as choke points for both axial gas flow and axial relocation of

fuel fragments during a LOCA. The mechanical restraint imposed by spacer grids would be fairly easy to model in FRAPTRAN-QT-1.5, simply by postulating restrictions on cladding radial deformation at the spacer grid axial positions. The uppermost spacers are of particular interest for axial gas flow modelling, since these spacers may restrict axial gas flow between the upper plenum and the ballooning part of the fuel rod. Likewise, spacers located at, and slightly below, the fuel rod axial peak power position are of importance for their restricting effect on cladding ballooning and fuel fragment axial relocation.

Acknowledgements

This work was carried out as part of a research project on fuel behaviour in LOCA conditions, funded by the Swedish Radiation Safety Authority (SSM) through research grant DNR SSM2022-3726. Many of the computational models in the extended versions of FRAPCON-4.0P1 and FRAPTRAN-1.5 that were applied in the presented analyses have been developed by Quantum Technologies AB in past research projects for SSM. The author gratefully acknowledges that the continuous funding provided by SSM over the years has been instrumental for the successful execution of this study.

Likewise, this study would not have been possible without the contributions from Ringhals AB and Vattenfall Nuclear Fuel AB, who provided detailed information on the design and operating histories for the high-burnup fuel rods analysed in this work. In addition, they also kindly provided the boundary conditions used for the supplementary fuel rod analyses in section 4.2.3. The author is grateful to Henrik Nylén and Anders Jonsson at Ringhals AB, as well as to Michael Söderström and Paul Blair at Vattenfall Nuclear Fuel AB, for their kind support and valuable input to the project.

5. References

1. *Nuclear fuel behaviour in loss-of-coolant accident (LOCA) conditions: State-of-the-art report,* 2009, Report NEA No. 6846, OECD Nuclear Energy Agency, Paris, France.
2. Geelhood, K.J., et al., *FRAPTRAN-2.0: A computer code for the transient analysis of oxide fuel rods,* 2016, Report PNNL-19400, Vol. 1 Rev. 2, Pacific Northwest National Laboratory, Richland, WA, USA.
3. Bratby, P.A.W., et al., *Fuel cladding failure criteria,* 2000, Report EUR 19256 EN, European Commission, Luxembourg.
4. Nagase, F., *Behavior of LWR fuel during loss-of-coolant accidents*, 2020. In: Comprehensive Nuclear Materials, R.J.M. Konings and R.E. Stoller, Editors. Elsevier. pp. 307-321.
5. Bales, M., *Establishing analytical limits for zirconium-alloy cladding material,* 2016, Regulatory Guide (draft) 1.224, U.S. Nuclear Regulatory Commission, Washington, DC, USA.
6. Oberländer, B.C. and W. Wiesenack, *Overview of Halden reactor LOCA experiments (with emphasis on fuel fragmentation) and plans,* 2014, Report IFE/KR/E-2014/001, Institute for Energy Technology, Kjeller, Norway.
7. Flanagan, M., et al., *Post-test examination results from integral, high-burnup, fueled LOCA tests at Studsvik Nuclear Laboratory,* 2013, Report NUREG-2160, U.S. Nuclear Regulatory Commission, Washington, DC, USA.
8. Magnusson, P., et al., *SCIP III Subtask 1.1: Fuel fragmentation, relocation and dispersal - Final summary report,* 2020, Report STUDSVIK-SCIP III-253 (STUDSVIK/N-19/105), Studsvik Nuclear AB, Nyköping, Sweden.
9. Capps, N., et al., *Integral LOCA fragmentation test on high-burnup fuel.* Nuclear Engineering and Design, 2020. 367: p. 110811.
10. Fedotov, P.V., et al. *LOCA test with high burnup VVER fuel in the MIR reactor*, 2015. In: Reactor Fuel Performance 2015 (TopFuel-2015), September 13-17, 2015, Zürich, Switzerland: European Nuclear Society, pp. 335-344.
11. Yan, Y., et al. *LOCA integral test results for high-burnup BWR fuel*, 2005. In: 2004 Nuclear Safety Research Conference, October 22-27, 2004, Washington, DC, USA: U.S. Nuclear Regulatory Commission, Report NUREG/CP-0192, pp. 111-158.
12. *Report on fuel fragmentation, relocation and dispersal,* 2016, Report NEA/CSNI/R(2016)16, OECD Nuclear Energy Agency, Paris, France.
13. Bales, M., et al., *Interpretation of research on fuel fragmentation, relocation and dispersal at high burnup,* 2021, Research Information Letter RIL 2021-13, U.S. Nuclear Regulatory Commission, Washington, DC, USA.
14. Capps, N., et al., *A critical review of high burnup fuel fragmentation, relocation, and dispersal under loss-of-coolant accident conditions.* Journal of Nuclear Materials, 2021. 546: p. ID 152750.

15. Arimescu, I., *Technical expert panel assessment of existing fuel fragmentation, relocation, and dispersal data: Current understanding and needs for future research,* 2022, White Paper EPRI 3002025542, Electric Power Research Institute, Palo Alto, CA, USA.
16. Wiesenack, W., *Safety significance of the Halden IFA-650 LOCA test results,* 2010, Report NEA/CSNI/R(2010)5, OECD Nuclear Energy Agency, Paris, France.
17. Meyer, R.O. and W. Wiesenack, *A critique of fuel behavior in LOCA safety analyses and a proposed alternative.* Nuclear Engineering and Design, 2022. 394: p. 111816.
18. Bánáti, J., *Simulation of a postulated Large Break LOCA transient at the Ringhals 4 NPP,* 2014, Research report commissioned by the Swedish Radiation Safety Authority, SSM 2014-1043-15, Chalmers University of Technology, Division of Nuclear Engineering, Gothenburg, Sweden.
19. *Ringhals-4,* 2024, IAEA Power Reactor Information System (PRIS) database, International Atomic Energy Agency, Vienna, Austria.
20. Bánáti, J., *Technical description of the RELAP5 model for the Ringhals 4 NPP,* 2013, Research report commissioned by the Swedish Radiation Safety Authority, SSM 2011-603-10, Appendix 4, Chalmers University of Technology, Division of Nuclear Engineering, Gothenburg, Sweden.
21. Jernkvist, L.O., *Modelling of fine fragmentation and fission gas release of UO_2 fuel in accident conditions.* European Physical Journal, Nuclear Sciences and Technologies, 2019. 5: p. ID 11.
22. Geelhood, K.J., et al., *FRAPCON-4.0: A computer code for the calculation of steady-state, thermal-mechanical behavior of oxide fuel rods for high burnup,* 2015, Report PNNL-19418, Vol. 1 Rev. 2, Pacific Northwest National Laboratory, Richland, WA, USA.
23. Blair, P., *Stavdata LOCA R4*. 2023, Vattenfall Nuclear Fuel AB, Stockholm, Sweden: E-mail, August 25, 2023.
24. Geelhood, K.J., et al., *FRAPTRAN-1.5: A computer code for the transient analysis of oxide fuel rods,* 2014, Report NUREG/CR-7023, Vol. 1, Rev. 1, Pacific Northwest National Laboratory, Richland, WA, USA.
25. Jernkvist, L.O. and A.R. Massih, *Models for axial relocation of fragmented and pulverized fuel pellets in distending fuel rods and its effects on fuel rod heat load,* 2015, Report SSM 2015:37, Swedish Radiation Safety Authority, Stockholm, Sweden.
26. Jernkvist, L.O., *Implementation of models for cladding high temperature metal-water reactions, phase transformation, creep and failure in the FRAPTRAN-1.4 computer program,* 2012, Report TR10-005V2, Quantum Technologies AB, Uppsala, Sweden.
27. Manngård, T. and A.R. Massih, *Modelling and simulation of reactor fuel cladding under loss-of-coolant accident conditions.* Journal of Nuclear Science and Technology, 2011. 48(1): pp. 39-49.
28. Jernkvist, L.O., *Models for axial gas flow and mixing in LWR fuel rods,* 2020, Research report SSM 2020:02, Swedish Radiation Safety Authority, Stockholm, Sweden.
29. Jernkvist, L.O., *Observed and corrected errors in source code and algorithms of FRAPTRAN-1.5,* 2015, Report TR15-002, Quantum Technologies AB, Uppsala, Sweden.

30. Knuutila, A., *Improvements on FRAPCON3/FRAPTRAN mechanical modelling,* 2006, Research report VTT-R-11337-06, VTT Technical Research Centre of Finland, Helsinki, Finland.
31. Jernkvist, L.O. and A.R. Massih, *Calibration of models for cladding tube high-temperature creep and rupture in the FRAPTRAN-QT-1.5 program,* 2021, Research report SSM 2021:04, Swedish Radiation Safety Authority, Stockholm, Sweden.
32. Jernkvist, L.O., *Cladding tube rupture under LOCA: Data and models for rupture opening size,* 2021, Research report SSM 2021:05, Swedish Radiation Safety Authority, Stockholm, Sweden.
33. Cathcart, J.V., et al., *Zirconium metal-water oxidation kinetics, IV: reaction rate studies,* 1977, Report ORNL/NUREG-17, Oak Ridge National Laboratory, Oak Ridge, TN, USA.
34. Jernkvist, L.O., *Computational assessment of LOCA simulation tests on high burnup fuel rods in Halden and Studsvik,* 2017, Report SSM 2017:12, Swedish Radiation Safety Authority, Stockholm, Sweden.
35. Jernkvist, L.O., *Computational analysis of SCIP III LOCA simulation tests OL1L04-LOCA1 and VUL2-LOCA1/2/3/4,* 2019, Report TR19-001 (STUDSVIK-SCIP III-257), Quantum Technologies AB, Uppsala, Sweden.
36. Jernkvist, L.O., *Computational analysis of SCIP LOCA simulation tests O3C1-LOCA and VUR1-LOCA1/2/3,* 2023, Report TR22-002, Quantum Technologies AB, Uppsala, Sweden.
37. Westman, A.E.R., *The packing of particles: Empirical equations for intermediate diameter ratios.* Journal of the American Ceramic Society, 1936. 19: pp. 127-129.
38. *Decay heat power in light water reactors,* 1994, Standard ANSI/ANS-5.1-1994, American Nuclear Society, La Grange Park, IL, USA.
39. *Appendix K decay heat standards,* 2002, Appendix 1 to Research Information Letter RIL-0202, U.S. Nuclear Regulatory Commission, Washington, DC, USA.
40. Thadani, A.C., *Revision of 10 CFR 50.46 and Appendix K,* 2002, Research Information Letter RIL-0202, U.S. Nuclear Regulatory Commission, Washington, DC, USA.
41. Rondinella, V.V., et al. *Measurement of gas permeability along the axis of a spent fuel rod*, 2015. In: 2015 Water Reactor Fuel Performance Meeting (TopFuel-2015), September 13-17, 2015, Zürich, Switzerland: European Nuclear Society, 2, pp. 217-225.
42. Montgomery, R. and R.N. Morris, *Measurement and modeling of the gas permeability of high burnup pressurized water reactor fuel rods.* Journal of Nuclear Materials, 2019. 523: pp. 206-215.
43. Wiesenack, W., et al. *Axial gas transport and loss of pressure after ballooning rupture of high burn-up fuel rods subjected to LOCA conditions*, 2008. In: International Conference on the Physics of Reactors 2008 (PHYSOR 08), September 14-19, 2008, Interlaken, Switzerland: R. Chawla, K. Mikityuk, and V.N. Dang, Editors, Paul Scherrer Institut, Switzerland, pp. 2987-2992.
44. Jernkvist, L.O., *Assessment of modelling approaches for axial gas flow inside LWR fuel rods,* 2022, Research report SSM 2022:09, Swedish Radiation Safety Authority, Stockholm, Sweden.

45. Khvostov, G., et al., *Some insights into the role of axial gas flow in fuel rod behaviour during the LOCA, based on Halden tests and calculations with the FALCON-PSI code.* Nuclear Engineering and Design, 2011. 241: pp. 1500-1507.

46. Jernkvist, L.O. and A.R. Massih. *Modelling axial relocation of fragmented fuel pellets inside ballooned cladding tubes and its effects on LWR fuel rod failure behaviour during LOCA*, 2015. In: 23rd International Conference on Structural Mechanics in Reactor Technology (SMiRT-23), August 10-14, 2015, Manchester, UK.

47. Jernkvist, L.O., et al. *Axial relocation of fragmented and pulverized fuel and its effects on fuel rod heat load during LOCAs*, 2015. In: Reactor Fuel Performance 2015 (TopFuel-2105), September 13-17, 2015, Zürich, Switzerland: European Nuclear Society, pp. 401-410.

48. Jernkvist, L.O., et al. *Computational assessment of axial fuel relocation in Halden IFA-650 LOCA tests*, 2016. In: Enlarged OECD Halden Programme Group Meeting, May 8-13, 2016, Fornebu, Norway.

49. Lee, J. and Y.S. Bang, *Effects of fuel relocation on fuel performance and evaluation of safety margin to 10CFR50.46c ECCS acceptance criteria in APR1400 plant.* Nuclear Engineering and Design, 2022. 397: p. 111945.

50. Zhang, J. and T. Drieu. *FRAPTRAN-TE-1.5 simulation of the Halden LOCA tests IFA-650.9 and 10: Impact of model options and assumptions*, 2022. In: TopFuel-2022: Light Water Reactor Fuel Performance Conference, October 9-13, 2022, Raleigh, NC, USA: American Nuclear Society, p. 3818.

51. Pastore, G., et al., *Analysis of fuel rod behavior during loss-of-coolant accidents using the BISON code: Fuel modeling developments and simulation of integral experiments.* Journal of Nuclear Materials, 2021. 545: p. ID 152645.

52. Turnbull, J.A., et al., *An assessment of the fuel pulverization threshold during LOCA-type temperature transients.* Nuclear Science and Engineering, 2015. 179: pp. 477-485.

53. Conover, W.J., *Practical nonparametric statistics*. 3rd ed. 1999, New York, NY, USA: John Wiley & Sons.

54. Pontillon, Y., et al. *Experimental and theoretical investigation of fission gas release from UO_2 up to 70 GWd/t under simulated LOCA type conditions: The GASPARD program*, 2004. In: 2004 International Meeting on LWR Fuel Performance (TopFuel-2004), September 19-22, 2004, Orlando, FL, USA: American Nuclear Society, pp. 490-499.

55. Greenquist, I. and N. Capps, *Effects of transient fission gas release on rod balloon burst behavior during a loss-of-coolant accident.* Annals of Nuclear Energy, 2024. 196: p. 110213.

56. *Nuclear Regulatory Commission: 10 CFR Parts 50 and 52: Performance-based emergency core cooling systems cladding acceptance criteria - Proposed rule.* Federal Register, 2014. 79(56): pp. 16106-16146.

57. Boutin, S. and S. Graff. *A new LOCA safety demonstration in France*, 2015. In: Reactor Fuel Performance 2015 (TopFuel-2015), September 13-17, 2015, Zürich, Switzerland: European Nuclear Society, pp. 384-393.

58. Uchida, M. and N. Otsubo, *Models of multi-rod code FRETA-B for transient fuel behaviour analysis (final version),* 1984, Report JAERI 1293, Japan Atomic Energy Research Institute, Tokai-mura, Naka-gun, Ibaraki-ken, Japan.

59. Uchida, M., *Application of a two-dimensional ballooning model to out-pile and in-pile simulation experiments.* Nuclear Engineering and Design, 1984. 77: pp. 37-47.

60. Glantz, T., et al., *DRACCAR: A multi-physics code for computational analysis of multi-rod ballooning, coolability and fuel relocation during LOCA transients Part one: General modeling description.* Nuclear Engineering and Design, 2018. 339: pp. 269-285.

61. Glantz, T., et al., *DRACCAR: A multi-physics code for computational analysis of multi-rod ballooning, coolability and fuel relocation during LOCA transients. Part two: Overview of modeling capabilities for LOCA.* Nuclear Engineering and Design, 2018. 339: pp. 202-214.

62. Freshley, M.D. and G.M. Hesson, *Summary results of the LOCA simulation program conducted in NRU,* 1983, Conference paper presented at the Eleventh Water Reactor Safety Research Information Meeting, Gaithersburg, MD, USA, October 24-28, 1983, Report PNL-SA-11536, Pacific Northwest Laboratory, Richland, WA, USA.

63. Esnoul, C., *IFA-650.16: LOCA test in-pile results,* 2019, Report HWR-1260, OECD Halden Reactor Project, Halden, Norway.

64. Oberländer, B.C. and H.K. Jensen, *Non-destructive post irradiation examination (PIE) of IFA-650.16, rod 16 after LOCA testing in the Halden reactor,* 2019, Report HWR-1241, OECD Halden Reactor Project, Halden, Norway.

65. Walton, L.A. and J.E. Matheson, *FUMAC - A new model for light water reactor fuel relocation and pellet-cladding interaction.* Nuclear Technology, 1984. 64: pp. 127-138.

66. Jernkvist, L.O., *Extended models in the FRAPTRAN-QT-1.5 program,* 2020, Report TR20-004V1, Quantum Technologies AB, Uppsala, Sweden.

67. Rosinger, H.E., *A model to predict the failure of Zircaloy-4 fuel sheating during postulated LOCA conditions.* Journal of Nuclear Materials, 1984. 120: pp. 41-54.

68. Söderström, M., *Termohydrauliska randvillkor för ett LBLOCA-fall för R4*. 2023, Vattenfall Nuclear Fuel AB, Stockholm, Sweden: E-mail, September 1, 2023.

Appendix A: Fuel rod thermal-mechanical boundary conditions

Except for some supplementary analyses, which are presented in Appendix D and summarized in section 4.2.3, all transient fuel rod thermal-mechanical analyses presented in this report are carried out with boundary conditions extracted from RELAP5/MOD3 results, reported for the limiting large-break LOCA case (case #24) in [18]. The boundary conditions, as well as the methods used for extracting them from Figures 9, 28 and 32 in [18], are described below.

A.1. Fuel rod axial power distribution

The fuel rod axial power distribution during the postulated LOCA was taken directly from Figure 9 in [18], which is reproduced in Fig. 29 below. The power distribution is peaked to the upper part of the core, with a peak-to-average ratio of 1.45 at z = 2.96 m. In the fuel rod analyses, this power distribution was held constant throughout the postulated LOCA.

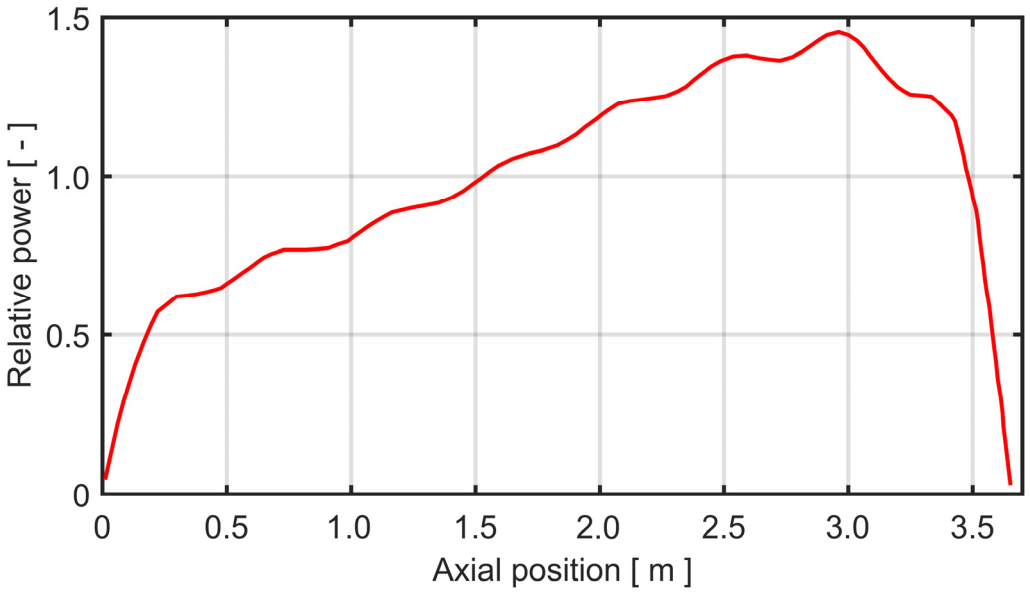

Fig. 29: Upper-peaked axial power distribution assumed during the postulated LOCA.

The power profile shown in Fig. 29 has a larger peaking factor than the end-of-life power distributions that were used in establishing the fuel rod pre-LOCA conditions with FRAPCON-QT-4.0P1. These end-of-life power distributions, which were specific to each of the fifty fuel rods, were also peaked to the upper part of the core, but their peak-to-average power ratios were around 1.35.

A.2. Coolant pressure and temperature

The coolant pressure applied in the transient fuel rod analyses is taken from Figure 32 in [18]. It is reproduced in Fig. 30 below, together with the corresponding saturated steam temperature. The saturated steam temperature, T_s, is calculated from the system pressure through a correlation. In the transient fuel rod analyses with FRAPTRAN-QT-1.5, T_s is used as the coolant bulk temperature, to which the cladding-to-coolant heat transfer coefficient, h, is referred. Hence, the cladding-to-coolant heat flux, J, is calculated from

$$J(t,z) \;=\; h(t,z)\big(\, T_{co}(t,z) - T_s(t) \,\big), \qquad (1)$$

where T_{co} is the cladding outer surface temperature. An exception is made for the first 500 ms of the accident, for which the saturation temperature cannot be used for representing the coolant bulk temperature. During this period, the pre-LOCA liquid coolant temperature, as calculated with FRAPCON-QT-4.0, was used instead of T_s as coolant reference temperature in eq. (1).

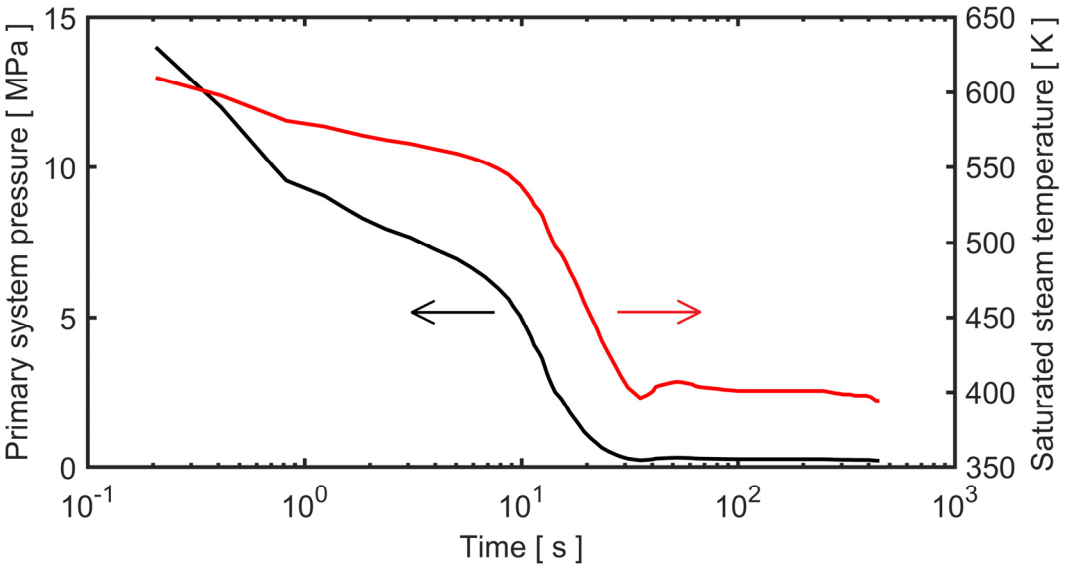

Fig. 30: Calculated primary system pressure (left, black line) and corresponding saturated steam temperature (right, red line) versus time during the LOCA.

A.3. Cladding-to-coolant heat transfer coefficient

In addition to the coolant pressure and temperature, the cladding-to-coolant heat transfer coefficient is needed to define the thermal-mechanical boundary conditions for the transient fuel rod analyses. No calculated results for the space-time evolution of h are presented in [18], but RELAP5/MOD3 results are presented for $T_{co}(t,z)$, calculated for the limiting case and the hottest fuel assembly. These results, which are reproduced in Fig. 31, have been used for determining the cladding-to-coolant heat transfer coefficient through reverse modelling with FRAPTRAN-QT-1.5. More precisely, the cladding-to-coolant heat flux $J(t,z)$ was first

calculated with FRAPTRAN-QT-1.5, using identical fuel rod conditions as in the RELAP5/MOD3 analysis as input and prescribing the cladding outer surface temperatures in Fig. 31 as Dirichlet boundary conditions to FRAPTRAN-QT-1.5. From the cladding-to-coolant heat flux obtained from these calculations, the corresponding heat transfer coefficient was then calculated through eq. (1). Due to fuel rod model differences between FRAPTRAN-QT-1.5 and RELAP5/MOD3, this calculated heat transfer coefficient was sometimes/somewhere slightly negative. These negative values were substituted with zero.

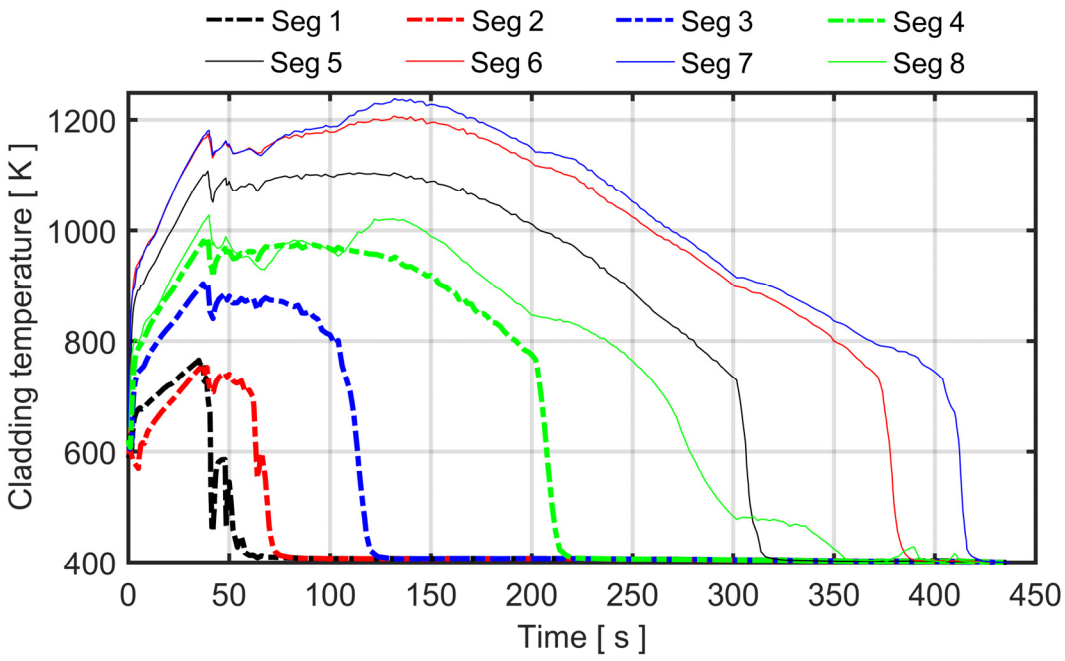

Fig. 31: Cladding temperatures calculated with RELAP5/MOD3 for the limiting large-break LOCA case in [18]. Results for eight equal-length axial segments, from rod bottom (Seg 1) to top (Seg 8).

The cladding-to-coolant heat transfer coefficients extracted from reported cladding temperatures for the eight axial segments by the reverse modelling with FRAPTRAN-QT-1.5 are shown in Fig. 32. The heat transfer coefficient typically drops rapidly from 35 kW$(m^2K)^{-1}$ at onset of LOCA to values close to zero during the blowdown phase. During refill, it stabilizes at 50-70 W$(m^2K)^{-1}$and increases gradually to about 100 W$(m^2K)^{-1}$ just before the cladding is re-wetted (quenched) by the raising water front. Upon re-wetting, the heat transfer coefficient increases rapidly to 3-8 kW$(m^2K)^{-1}$.

In all transient fuel rod analyses with FRAPTRAN-QT-1.5 presented in the main part of this report, the heat transfer coefficients shown in Fig. 32 are used together with the saturated steam temperature shown in Fig. 30 to define Neumann-type thermal boundary conditions for the postulated LOCA. The analyses are performed with the fuel rods discretized into 36 equal-length axial segments. The heat transfer coefficient for each of these segments is obtained by interpolation in the results calculated for 8 equal-length axial segments, as shown in Fig.

32, using an improved interpolation method [29]. The interpolation leads to rather anomalous results for h during re-wetting in intermediate axial positions, i.e. in positions halfway between those for which h has been determined. The reason is that the interpolation cannot capture the dramatic change in h as the quench front progresses axially along the fuel rod. However, this has a negligible effect on the calculated fuel rod behaviour, since the temperature is generally low (~750 K) when the re-wetting occurs; see Fig. 31.

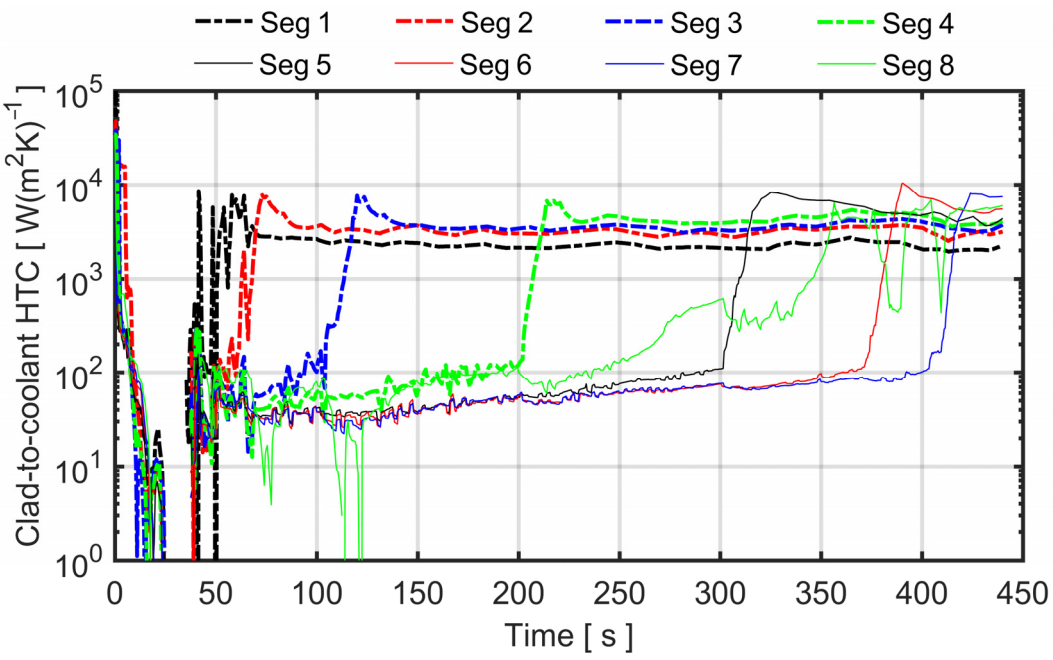

Fig. 32: Cladding-to-coolant heat transfer coefficients extracted from the calculated cladding temperatures in Fig. 31 by reverse modelling with FRAPTRAN-QT-1.5. Results for eight equal-length axial segments, from rod bottom (Seg 1) to top (Seg 8).

Finally, it should be remarked that the cladding temperatures shown in Fig. 31 are calculated for a fresh (un-irradiated) fuel rod with a rod average pre-LOCA LHGR of 21.9 kWm^{-1} [18], which means that the extracted heat transfer coefficients in Fig. 32 apply first and foremost to these conditions. In our transient fuel rod analyses with FRAPTRAN-QT-1.5, the extracted heat transfer coefficients are applied to fifty high-burnup fuel rods with pre-LOCA ALHGR between 2.6 and 19.2 kWm^{-1}. As shown in this report, the most interesting rods with regard to thermal-mechanical behaviour are those with pre-LOCA ALHGR above about 15 kWm^{-1}. The extracted heat transfer coefficients in Fig. 32 are deemed to be adequate for these power levels, but less appropriate for low-power fuel rods.

Appendix B: Specific models used in analyses with FRAPTRAN-QT-1.5

B.1. Axial transmissivity of gas

An important parameter in the applied model for axial gas flow and mixing [28] is the axial transmissivity (or permeability) of gas. From axial gas flow experiments, this parameter is known to depend on the local crack density in the fuel pellets and on the local width of the pellet-cladding gap [44]. The model in FRAPTRAN-QT-1.5 uses the following expression for calculating the axial transmissivity $\mathcal{T}$ [m^4] from these local conditions:

$$\mathcal{T} = \frac{2A_{cs}D_h^2}{\mathrm{Hg}}, \tag{2}$$

where Hg [-] is the Hagen number, A_{cs} [m^2] is the total cross-sectional flow area made up of the pellet-cladding gap and the pellet cracks, and D_h [m] is the hydraulic diameter of the flow channel. In FRAPTRAN-QT-1.5, the total cross-sectional flow area is calculated from

$$A_{cs} = A_{gap} + A_{cr} = \pi(2R_p + w_g)w_g + \pi(R_p^2 - (R_p - \delta_r)^2), \tag{3}$$

where R_p [m] is the deformed radius of the fuel pellet, w_g [m] is the pellet-cladding radial gap width, and δ_r [m] is the irreversible radial relocation of the fuel pellet surface, caused by pellet cracking. All these properties are calculated versus time and axial position by FRAPTRAN-QT-1.5. The hydraulic diameter is calculated through the well-known relation

$$D_h = 4A_{cs}/P_w, \tag{4}$$

where the wetted perimeter P_w [m] of the flow channel is estimated from

$$P_w = P_{w\,gap} + P_{w\,cr} = 2\pi(R_p + R_{ci}) + 2N_{cr}R_p. \tag{5}$$

Here, R_{ci} [m] is the cladding inner radius and N_{cr} [-] is the number of radial cracks in the fuel pellet. This number is calculated through a correlation with burnup and peak LHGR experienced by the fuel pellet during its in-reactor lifetime [25, 65].

The Hagen number in eq. (2) is set to 96. With this choice of Hg, the computational model reproduces exact analytical solutions to Hagen-Poiseuille flow in annular concentric ducts, i.e. cases with un-cracked pellets, $N_{cr} = A_{cr} = 0$. Finally, the transmissivity can be transformed to axial permeability κ [m^2] through

$$\kappa = \frac{\mathcal{T}}{\tilde{A}} = \frac{\mathcal{T}}{\pi R_{ci}^2}. \tag{6}$$

where $\tilde{A}$ [m^2] is the gross cross-sectional area inside the cladding tube [44].

B.2. Cladding high-temperature burst stress

Cladding high-temperature burst (rupture) may in FRAPTRAN-QT-1.5 be modelled by any of nine different failure criteria that are available as options in the program [66]. The criteria are defined as thresholds for either cladding hoop strain or hoop stress. These thresholds depend primarily on cladding temperature, but they may also account for heating rate and oxygen concentration in the cladding metal. They are empirical, and most of them are based on burst tests on Zircaloy cladding [66].

For the fuel rod analyses presented in this report, we apply the stress-based failure criterion described in [31]. This criterion originates from Rosinger's well-known criterion for Zircaloy-4 [67]. In a recent research project [31], this criterion was re-calibrated against a more extensive data base, including burst tests and LOCA simulation tests on Zircaloy-4, Zircaloy-2 and first generation ZIRLO cladding. Moreover, the calibration was done together with other models for cladding high-temperature behaviour in FRAPTRAN-QT-1.5, e.g. for cladding creep and oxidation. This integral-type calibration ensures that models used for different high-temperature phenomena in FRAPTRAN-QT-1.5 work well together.

According to the applied criterion, cladding failure is assumed to occur if the cladding Cauchy (true) hoop stress exceeds a threshold stress, σ_b [Pa], which is correlated to temperature, T [K], and cladding metal layer excess oxygen concentration, x_M [weight fraction], through

$$\sigma_b(T, x_M) \quad = \quad A_b e^{-B_b T} e^{-(x_M/C_b)^2} . \tag{7}$$

The metal layer excess oxygen concentration is the oxygen that has diffused into the metal layer as a result of high-temperature metal-water reactions. In the presented analyses with FRAPTRAN-QT-1,5, x_M is calculated versus space and time through Cathcart-Pawel's high-temperature oxidation model [33] and does not include the as-fabricated oxygen content of the cladding material, nor the oxygen that forms the cladding oxide layer. Finally, A_b, B_b and C_b are model parameters that depend on the phase composition of the cladding material. For simplicity, they are correlated to temperature rather than the calculated phase composition in FRAPTRAN-QT-1.5; see Table 7.

Table 7: Parameters used for the cladding burst stress criterion defined in eq. (7).

Temperature range **[K]**	A_b **[Pa]**	B_b **[K^{-1}]**	C_b **[-]**
873 – 1075	7.3757×10^{10}	5.9298×10^{-3}	5.888×10^{-4}
1075 – 1250	5.1513×10^{12}	9.8798×10^{-3}	5.888×10^{-4}
1250 – 1873	2.3301×10^{7}	3.4814×10^{-5}	5.888×10^{-4}

B.3. Fuel fragment packing fraction

In axial segments of the fuel rod where the fuel pellet column has collapsed into a particle bed, the packing fraction of fuel fragments is calculated trough a model proposed by Westman [37]. The model, which is fully described in [25], considers a binary mixture of large (L) and small (S) particles with known mass fractions x^L and $x^S = 1 - x^L$, respectively. The packing fractions of mono-component beds of the large and small particles are also assumed to be known and denoted ϕ^L and ϕ^S. The overall packing fraction of the binary mixture, ϕ, can then be estimated from Westman's original model through the relation

$$a^2 + 2Gab + b^2 = 1, \tag{8}$$

where

$$a = \frac{\phi^S \left(\phi^L - x^L \phi \right)}{\phi \phi^L}, \tag{9}$$

$$b = \frac{\phi^S \phi^L - \phi \phi^L \left(x^S + x^L \phi^S \right)}{\phi \phi^S \left(1 - \phi^L \right)}, \tag{10}$$

and G is a parameter that depends on the differences in particle shape and size between the two components of the mixture. This parameter is in our model estimated through general expressions, based on assumed particle characteristics [25].

From earlier analyses of LOCA simulation tests, we have noticed that Westman's original model tends to overestimate the fragment packing fraction when it is combined with our model for fuel fine fragmentation and applied to high burnup fuel rods with x^S in the range from 0.2 to 0.5. For this reason, we use a modified expression for the fragment packing fraction, defined by

$$\tilde{\phi} = \frac{1}{4} \left(\phi^S + \phi^L + 2\phi \right), \tag{11}$$

where ϕ is the packing fraction calculated by Westman's original model. The modification in eq. (11) reduces the calculated packing fraction for mixtures of small and large fragments, as shown in Fig. 33. The example in Fig. 33 is calculated with the parameters in Table 2 used for Westman's original model, together with an assumed size of large fragments of 1.85 mm. This fragment size is typical for the high-burnup fuel studied here: it depends on the past operating life of the fuel [25]. We note that the modified model yields packing fractions that are in line with those measured on relocated fuel with a pellet burnup around 65 MWd(kgU)$^{-1}$ in experiments carried out within SCIP III; see Figure 12 in [13].

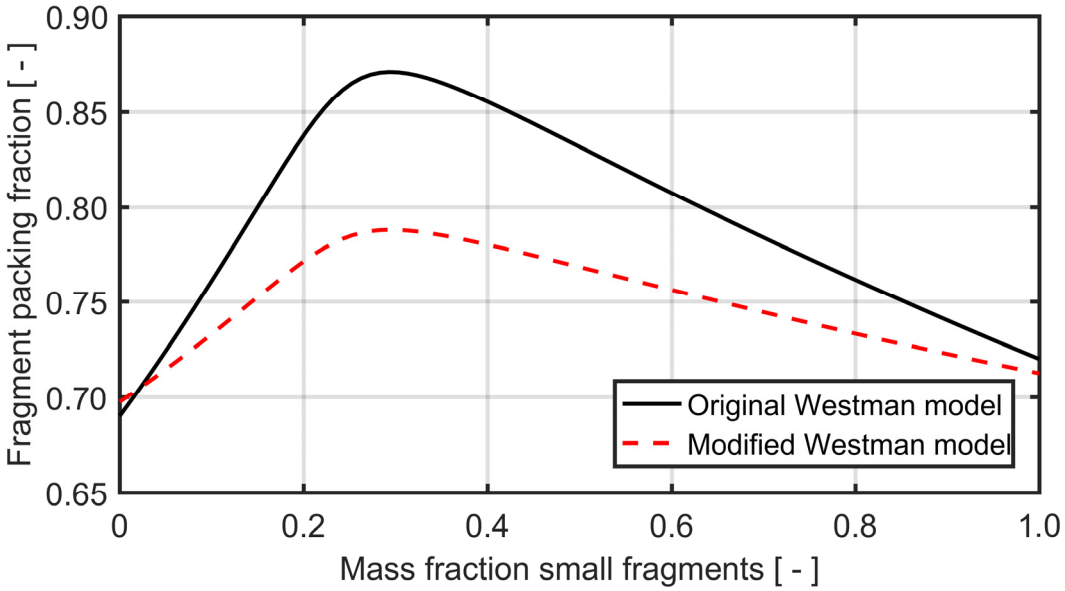

Fig. 33: Fuel fragment packing fraction, calculated with the original (ϕ) and modified ($\tilde{\phi}$) Westman model by use of the parameters in Table 2 and an assumed size of large fragments of 1.85 mm, which is typical for the fuel studied here.

The Swedish Radiation Safety Authority (SSM) works proactively and preventively with nuclear safety, radiation protection, nuclear security, and nuclear non-proliferation to protect people and the environment from the harmful effects of radiation, now and in the future.

You can download our publications from www.stralsakerhetsmyndigheten.se/en/publications. If you need alternative formats such as easy-to-read, Braille or Daisy, contact us by email at registrator@ssm.se.

Strålsäkerhetsmyndigheten
SE-171 16 Stockholm
+46 (0) 8-799 40 00
www.stralsakerhetsmyndigheten.se
registrator@ssm.se

E-print AB, 2024